Liquid-Phase Alkali-Doping of Individual Carbon Nanotube Field-Effect Transistors

Konsta Hannula

Master's Thesis
University of Jyväskylä, Department of Physics
31.5.2012
Supervisor: Markus Ahlskog

Preface

The present work was carried out between June 2010 and February 2012 in the Molecular Technology research group at the Department of Physics in the University of Jyväskylä.

First, I would like to thank my supervisor Professor Markus Ahlskog and Dr. Andreas Johansson for providing me with an interesting research topic and advice throughout the years I have been in this group. I also wish to thank Mr. Peerapong Yotprayoonsak for help and collaboration during the experimental work. I thank also the other members of the group and all the people in the Nanoscience Center for valuable advice especially with the equipment needed in the experimental work. I would like to thank Dr. Tanja Lahtinen for her support in the chemistry part of this work and spec. lab. tech. Reijo Kauppinen for help with making the flow chamber of glass.

I would also like to thank the Foundation of Taru, Ilmari, and Pentti Manninen for financial support for the writing part of this thesis.

Finally, I wish to thank my parents, siblings, and all my friends for their support. Special thanks belong to my wife Anne and my daughter Ellen for their love, support and patience during this work.

Jyväskylä, May 2012

Konsta Hannula

Tiivistelmä

Hiilinanoputket ovat todella herkkiä niiden lähiympäristössä tapahtuville muutoksille, joten niiden virrankuljetusominaisuuksia pystytään suhteellisen helposti muokkaamaan. Aromaattiset molekyylit esimerkiksi vuorovaikuttavat hiilinanoputken kanssa $\pi - \pi$ -vuorovaikutusten välityksellä, jolloin molekyylien ja hiilinanoputken välillä voi tapahtua varausten siirtoa. Varausten siirtyminen taas muuttaa hiilinanoputken Fermi-tasoa ja vaikuttaa putken virrankuljetusominaisuuksiin. Myös atomeja voidaan kiinnittää hiilinanoputken seinämiin esimerkiksi sähköstaattisten vuorovaikutusten avulla, jolloin varausten siirron ja Fermi-tason muutoksen myötä putken virrankuljetusominaisuudet muuttuvat. Näiden esimerkkien kaltaista hiilinanoputkien sähköisten ominaisuuksien kemiallista muuttamista kutsutaan tavallisesti ”douppaukseksi”. Hiilinanoputkitransistorit, joiden elektrodit on tehty tavanomaisista metalleista, kuten kullasta tai palladiumista, ovat yleensä p-tyyppiä. Douppaus on yksi keino saada myös n-tyypin hiilinanoputkitransistoreja, joita tarvitaan loogisissa piireissä. Höyrystettyjä alkalimetalleja on yleisesti käytetty hiilinanoputkitransistoreiden n-tyypin douppaukseen, ja muutos p-tyypistä n-tyyppiin on vahvistettu hiilinanoputken virrankuljetusominaisuuksia mittaamalla. Samankaltaisia suoria sähköisiä mittauksia ei ole ennen tehty yksittäisille hiilinanoputkille, jotka on altistettu liuosfaasissa olevalle alkalimetallille. Tästä johtuen tämän gradun päätarkoitus oli tutkia liuosfaasissa olevan alkalimetallin douppausvaikutuksia yksittäisten hiilinanoputkien virrankuljetusominaisuuksiin. Alunperin puhtaasti p-tyypin hiilinanoputkitransistorit havaittiin muuttuvan puhtaasti n-tyypin transistoreiksi, jotka myös säilyttivät melko hyvin alkuperäiset ominaisuutensa, kuten esimerkiksi ON/OFF -suhteensa ja hilariippuvaisen virran kulmakertoimensa transitioalueella. Hiilinanoputkitransistorit ovat erittäin lupaavia pohjarakenteita nanosensorisovelluksille johtuen hiilinanoputkien herkkyydestä lähiympäristön muutoksille. Tutkimuksen toisena tavoitteena oli löytää douppausprosessin aikariippuvuus ja näin ollen testata hiilinanoputkitransistorin toimintaa nanosensorina. Sopivalla alkaliliuoksen laimennoksella hiilinanoputkitransistori saatiin doupattua kokonaan muutamassa tunnissa ja alkalikationien tarrautuminen hiilinanoputken pinnalle havaittiin yli kolmen kertaluvun virran muutoksena.

Avainsanat: Hiilinanoputki, transistori, alkali, douppaus, sensori

UNIVERSITY OF JYVÄSKYLÄ
Faculty of Mathematics and Science

Author:	Konsta Hannula
Topic of the Master's Thesis:	Liquid-Phase Alkali-Doping of Individual Carbon Nanotube Field-Effect Transistors
Supervisor:	Markus Ahlskog
Degree:	Master of Science
Department:	Department of Physics
Major subject:	Physics
Degree Programme:	MDP in Nanoscience
Year of Completing the Master's Thesis:	2012
Pages:	85

Abstract

Carbon nanotubes (CNTs) are very sensitive to changes in their environment, thus their electronic transport properties can be quite easily modified. For example, when aromatic molecules interact with a CNT via $\pi - \pi$ interactions, there can occur charge transfer between the CNT and the absorbed aromatic molecules. This shifts the Fermi level of the CNT and changes its electronic transport properties. Atoms can also be attached to the sidewalls of a CNT for example via electrostatic interactions. As in the previous case, the charge transfer and the shift of the Fermi level change the electronic transport properties of the CNT. These kind of chemical tuning is usually called "doping". Carbon nanotube field-effect transistors (CNT FETs) with electrodes made of conventional metals, such as gold or palladium, have usually p-type behavior. Doping offers one way to obtain n-type CNT FETs needed in logic circuits. Vaporized alkali metals have been commonly used for n-type doping of CNT FETs, and the reversal from p- to n-type behavior has been confirmed by electronic transport measurements. Same kind of direct electrical measurements have not been done earlier for individual carbon nanotubes exposed to liquid-phase alkali solution. Thus the main objective of this thesis was to study the effects of liquid-phase alkali-doping to the electronic transport properties in individual carbon nanotubes. Originally clear p-type CNT FETs were found to change to clear n-type while keeping quite well their

initial characteristics, such as ON/OFF ratios and subthreshold slopes. Due to the sensitivity of CNTs to changes in their environment, CNT FETs are commonly acknowledged as a potential base structure for nanosensor applications. Thus another aim of this study was to test the sensor-like behavior of CNT FETs and find out the time dependence of the doping process. With a suitable dilution of alkali solution, a CNT FET was completely doped in a few hours and the attachment of alkali cations was detected with a current response changing more than three orders of magnitude.

Keywords: Carbon nanotube, field-effect transistor, alkali, doping, sensor

Contents

Introduction

The discovery of carbon nanotubes in 1991 launched a new fastly growing reseach field. Carbon nanotubes are a few nanometers thick, about 50 000 times thinner than a human hair, hollow carbon cylinders with micrometric length, and they have excellent physical and chemical properties. They can be used in diverse applications from extra strong composites to ultra sensitive nanosensors. They are also supposed to be a potential building block for a new generation's high-performance integrated electronic devices that will allow the electronics industry to overcome the problems with linewidth reduction and to fill the well-known Moore's law of miniaturization of the size of electronic components for another two decades.

One of the most known and researched application of carbon nanotubes is the carbon nanotube field-effect transistor (CNT FET) that resembles conventional field effect transistor, but the channel between source and drain electrodes is replaced with semiconducting carbon nanotube. Carbon nanotubes are very sensitive to changes in their environment, so CNT FETs can be used as base structures for nanosensors.

The electronic properties of carbon nanotubes can be quite easily tuned for more demanding applications. This kind of tuning is usually called "doping". In many cases, traditional preparation methods of CNT FETs do not produce themselves the properties which are needed in more complex applications. One good example is the type of semiconducting CNT FET: when conventional metals (palladium, gold, ...) are used for contact electrodes, the prepared CNT FET has mostly p-type behavior. Logic circuits need both n- and p-type FETs, so doping offers one way to obtain needed n-type CNT FETs.

Alkali metal vapors are commonly used for n-type doping of CNT FETs, and the reversal from p- to n-type behavior has been confirmed by electronic transport measurements [1–3]. Same kind of direct electrical measurements have not been done earlier for individual CNTs exposed

to liquid-phase alkali solution, so the main objective of this thesis is to study the effects of liquid-phase alkali-doping to the electronic transport properties in individual CNT FET. In addition, the sensor properties of CNT FET are tested by monitoring the doping process in real time.

It is possible to dissolve alkali metals, such as lithium, in a solution containing naphthalene and the polar solvent tetrahydrofuran (THF). This alkali solution has been proved to tune the electronic structure of CNT by monitoring the optical properties of thin film CNT samples [4]. The same solution has been found to change the electrical conductivity of the buckypaper sample as well [5]. Although these studies are quite different from direct electrical measurements, they support the hypothesis, that this alkali solution really dopes CNT FETs.

Chapter 1 presents theoretical background of this thesis concentrating on carbon nanotubes and carbon nanotube field-effect transistors. In addition, the usage of CNT FETs in sensor applications is discussed. Chapter 2 describes the previous studies, presenting shortly the background and properties of doping alkali solution, and how the electronic properties of carbon nanotubes can be consciously tuned (“doped”) . The experimental techniques of this study are discussed in Chapter 3. It contains detailed description of the multistep process of CNT FET fabrication, and the preparation of alkali solution. Chapter 4 presents measurement procedures and results. Chapter 5 sums up the whole study and the main results, presenting also some future prospects and possible applications based on the findings of this study.

Chapter 1

Theory

1.1 Overview of Carbon Nanotubes

The carbon nanotube is a honeycomb lattice of carbon atoms rolled into a hollow cylinder with nanometric diameter and micrometric length. Carbon nanotubes possess extremely interesting mechanical, electrical, chemical, and optical properties, stimulating researchers in universities and industry to study them and to develop exiting applications from them. In this section, carbon as the most diverse material in nature is shortly introduced. Some common synthesis methods and applications of carbon nanotubes are discussed, too.

1.1.1 Diversity of Carbon

Carbon is one of the most versatile elements due to its electronic configuration $1s^2 2s^2 sp^2$ which can form three different types of hybridizations: sp, sp^2 and sp^3. These hybridizations enable carbon to create strong covalent single, double, and triple bonds with itself and with other atoms creating a vast amount of molecules with interesting properties. All living organisms are based on carbon chemistry and there is an entire scientific discipline, organic chemistry, which studies the chemistry of carbon-based compounds. [6]

All-carbon crystalline structures are unique in many ways and they have been a very hot topic in science during the last half a century. A few decades ago only two types of all-carbon crystalline structure, the naturally occurring allotropes diamond and graphite, were known (see Figure 1.1) [7]. Very small diameter carbon filaments were synthesized

in the 1970's and 1980's [8,9], but no detailed systematic studies of these filaments were done at that time.

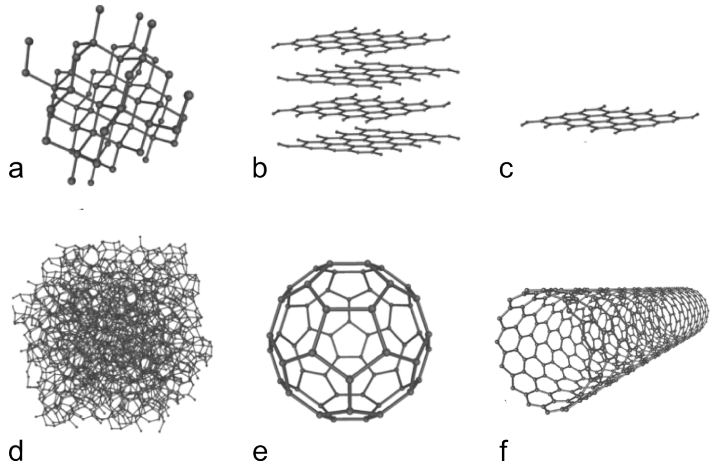

Figure 1.1: Some common allotropes of carbon: a) diamond, b) graphite, c) graphene, d) amorphous carbon, e) Buckminsterfullerene, and f) single-wall carbon nanotube. Adapted from ref. [10]

The discovery of spherical carbon structures, fullerenes, in 1985 [11] stimulated researchers to study more closely very narrow carbon filaments. One assumption based on this discovery stated that a single-wall carbon nanotube (SWCNT) might be a limiting case of a fullerene molecule. In this thesis, the word "CNT" refers to SWCNT unless otherwise noted. In 1991 *Sumio Iijima* discovered multi-wall carbon nanotubes (MWCNTs) by using High-Resolution Transmission Electron Microscopy (HRTEM) [12]. About two years later *Iijima* et al. and *Bethune* et al. independently reported the synthesis of single-wall carbon nanotubes (see Figure 1.2) [13, 14]. *Andrei Geim* and *Kostya Novoselov* continued pioneering work with carbon allotropes, when they succeeded to peel atomically thin layers of graphene from lumps of graphite by using sticky tape in 2004. This discovery completed the dimensionalities of carbon allotropes to extend from 0D to 3D (0D fullerenes, 1D CNTs, 2D graphene and 3D graphite). The number of publications per year in 2010 proves the wide interest in these three allotropes of carbon: carbon nanotubes have beyond 8000 publications, graphene about 3000, and fullerenes about 1500 publications [15].

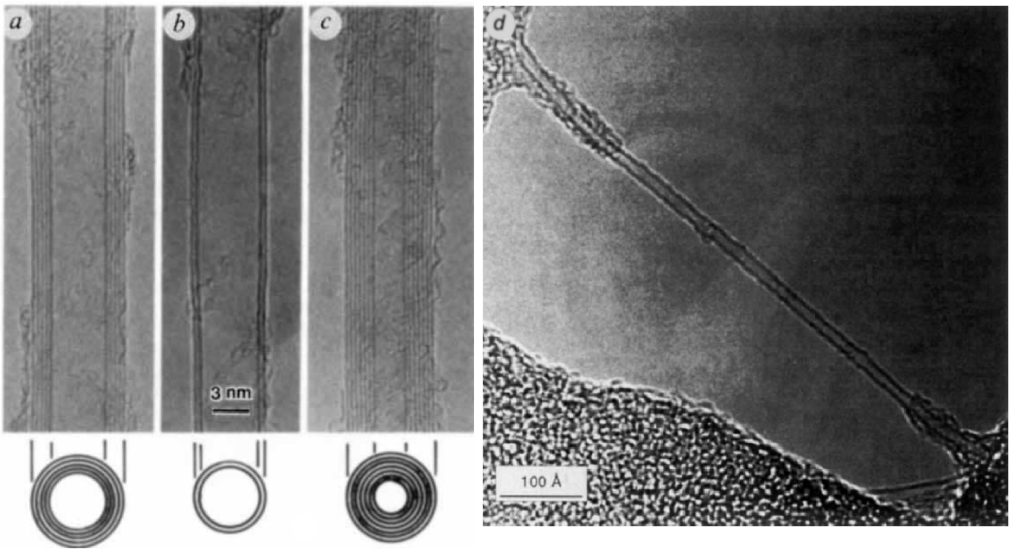

Figure 1.2: HRTEM images of Iijimas MWCNTs with a) five shells, b) two shells, and c) seven shells. TEM image of SWCNT in d) is taken by Bethune et al. Adapted from ref. [12, 14].

1.1.2 Synthesis

The method of preparation and further processing decides the structure, morphology and properties of carbon nanotubes, thus many different synthetic methods have been developed to produce carbon nanotubes with desired properties for specific scientific or technological purposes. The main challenges are the development of cheap and effective mass production methods, selective production (for controlling physical and electrical properties of nanotubes), the organization of the produced nanotubes on a flat surface, and the understanding of the fundamentals of the growth processes. [16]

The three main methods for the preparation of high-quality single-wall carbon nanotubes with high yield are arc discharge, laser ablation, and chemical vapor deposition (CVD). In the arc discharge method a discharge is produced between the electrodes (carbon rods separated by approximately 1 mm), which vaporises the surface of one carbon electrode, and the nanotubes start to form on the other electrode. The discharge is usually carried out at a voltage of 20 V, with a current of 50 to 100 A. [17]

In the laser ablation process the graphite target with a mixture of, for example Cobalt and Nickel as a catalyst is vaporized by a pulsed laser in

a high temperature chamber. Argon (or other inert gas) flows through the growth chamber and carries the grown nanotubes downstream to a cooled collector. For the growth of CNTs, a metal catalyst is needed both in the arc-discharge and in the laser ablation methods. [18]

The mechanism of nanotube growth in the arc-evaporation and laser ablation methods is still under debate, but many theories suggest that the precursor is a fullerene soot type material which contains the seeds for nanotube growth (see Figure 1.3). [18]

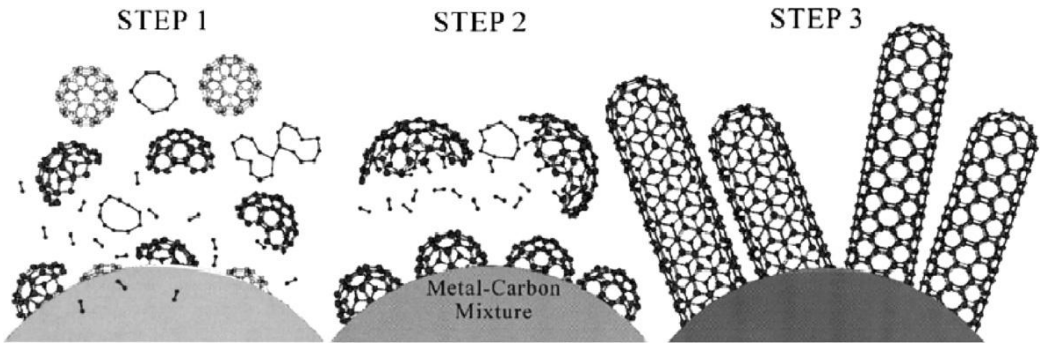

Figure 1.3: A model for CNT growth. In Step 1, carbon clusters with fullerene-like structures form, while some of carbon dissolves in metal particles. In Step 2, the metal particles are saturated with carbon and their surfaces start to cover with carbon clusters. In the last step, CNTs grow out from the metal particles. [18]

In the chemical vapor deposition the decomposition of a gaseous or volatile compound of carbon (e.g. methane) is catalyzed by metallic nanoparticles. Formed free carbon dissolves into these liquid metal clusters, and when the metal-carbide clusters are supersaturated in carbon, nanotubes start to grow from carbon islands precipitated on the cluster surface. [19]

1.1.3 Applications

As mentioned earlier, the versatile properties of carbon nanotubes provide an interesting building block for future applications. Carbon nanotubes are one of the stiffest and lightest materials known with a tensile strength measured up to 63 Gpa [20] and a Young modulus around 1 TPa [21]. The electrical properties of CNTs are impressive as well. For example, very short CNTs have ballistic transport [22], and a metallic carbon nanotube can carry a current density up to ~10^9 A/cm^2 (over three orders of magnitude bigger than copper) [23]. These excellent electronic properties with the

unique chemical properties (e.g. high chemical stability) are very useful in sensor applications [24]. The high strength and low density of CNTs open possibilities to use them for thin conducting sheets [25] and composite materials [26]. The high aspect ratio (length divided by diameter) of CNTs is ideal for scanning probe microscopy [27] while the large surface to volume ratio is beneficial for hydrogen storage in fuel cells [28].

1.2 Properties of Carbon Nanotubes

A carbon nanotube can be described as a graphene sheet rolled into a cylindrical form. Due to this, many properties of carbon nanotubes can be derived from the properties of graphene. This section bases mainly on the extensive review in [22] describing the atomic structure of carbon nanotubes and introducing their electronic and transport properties.

1.2.1 Atomic Structure of Carbon Nanotubes

The microscopic structure of CNT is similar to a rolled graphene strip, so the unit vectors of a graphene honeycomb lattice, $\mathbf{a}_1$ and $\mathbf{a}_2$, are usually used to describe the structure of CNTs (see Figure 1.4):

$$\mathbf{a}_1 = \left(\frac{\sqrt{3}}{2}; \frac{1}{2}\right) a \tag{1.1}$$

$$\mathbf{a}_2 = \left(\frac{\sqrt{3}}{2}; -\frac{1}{2}\right) a. \tag{1.2}$$

where a is the lattice constant of the graphene sheet: $a = \sqrt{3}a_{cc}$. The C-C bond length $a_{cc} \approx 1.42$ Å, so $a \approx 2.46$ Å. The chiral vector ($\mathbf{C}_h$), which connects two crystallographically equivalent sites (A and A') on the graphene sheet, tells us how the graphene strip is rolled up and determines the circumference of the CNT. It is always an integer multiple of vectors $\mathbf{a}_1$ and $\mathbf{a}_2$:

$$\mathbf{C}_h = n\mathbf{a}_1 + m\mathbf{a}_2 = (n, m), \tag{1.3}$$

where the chiral indices (n, m) define the exact atomic structure and chiral symmetry of a particular nanotube. Nanotubes have specific names depending on their chiral indices: nanotubes having $(n, 0)$ are called

zigzag tubes, (n, n) are armchair tubes and others with $(n, m \neq n \neq 0)$ are chiral tubes. The chiral indices determine also the electronic properties of the nanotubes.

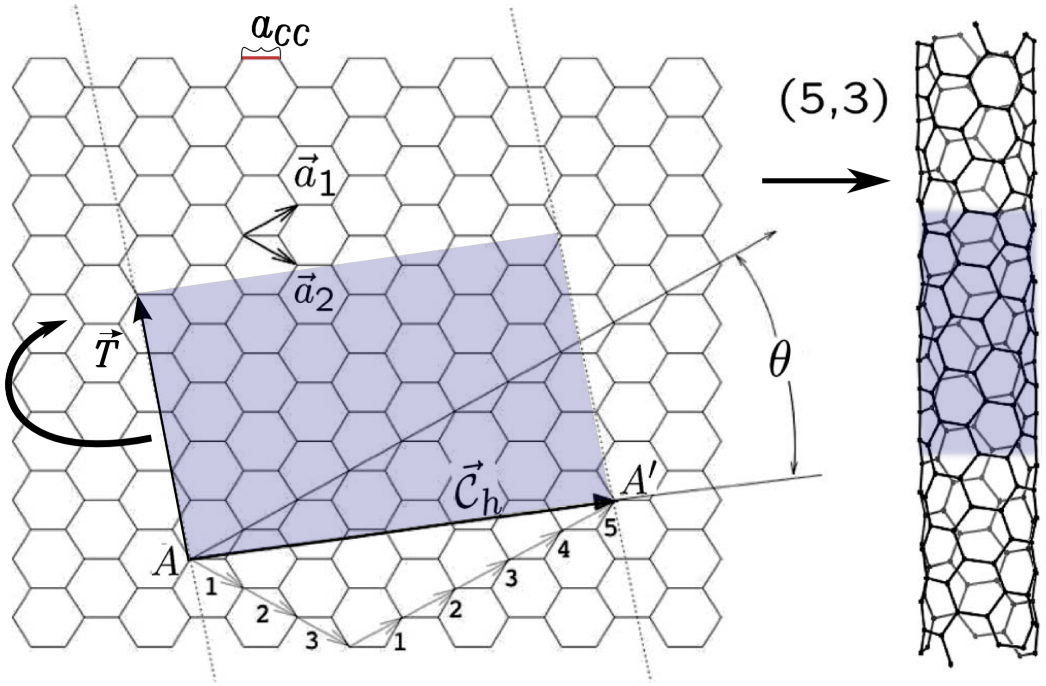

Figure 1.4: Graphene honeycomb lattice with unit vectors $\mathbf{a}_1$ and $\mathbf{a}_2$. a_{cc} is the C-C bond length. The translational vector $\mathbf{T}$ is parallel to formed nanotube axis. The chiral indices (5,3) for the tube are the integers multiplying the unit vectors in the chiral vector $\mathbf{C}_h = 5\mathbf{a}_1 + 3\mathbf{a}_2$. The chiral angle θ is the angle between the $\mathbf{C}_h$ vector and the $\mathbf{a}_1$ vector. The light blue area describes the unit cell of the nanotube. Adapted from ref. [22].

The chiral vector is always perpendicular to the tube axis and since the length of the chiral vector is the circumference of the nanotube, the diameter of the tube is

$$d = \frac{|\mathbf{C}_h|}{\pi} = \frac{a}{\pi}\sqrt{n^2 + nm + m^2}, \tag{1.4}$$

The chiral angle θ is the angle between $\mathbf{C}_h$ and $\mathbf{a}_1$ (zigzag direction of the graphene sheet). It can be written by the aid of the unit vectors as

$$\theta = cos^{-1}\frac{\mathbf{C}_h \cdot \mathbf{a}_1}{|\mathbf{C}_h||\mathbf{a}_1|} = cos^{-1}\left(\frac{2n + m}{2\sqrt{n^2 + nm + m^2}}\right). \tag{1.5}$$

The hexagonal symmetry of the graphene lattice limits the chiral angle on the range $0° \leq \theta \leq 30°$.

The chiral vector $\mathbf{C}_h$ and the translational vector $\mathbf{T}$ are perpendicular to each other, and they define the unit cell of the nanotube (see Figure 1.4). The translation vector is defined as

$$\mathbf{T} = t_1\mathbf{a}_1 + t_2\mathbf{a}_2 = (t_1, t_2), \tag{1.6}$$

where $t_1, t_2 \in \mathbb{N}$.

The unit cell of graphene consists of two atoms (see Figure 1.5), and the whole graphene lattice can be covered by multiplying it. The Fourier transform of formed Bravais lattice produces the reciprocal lattice with unit vectors $\mathbf{b}_1$ and $\mathbf{b}_2$. They can be calculated from the unit vectors of the direct lattice resulting

$$\mathbf{b}_1 = \left(\frac{1}{2}; \frac{\sqrt{3}}{2}\right) b \tag{1.7}$$

$$\mathbf{b}_2 = \left(\frac{1}{2}; -\frac{\sqrt{3}}{2}\right) b, \tag{1.8}$$

where $b = \frac{4\pi}{a\sqrt{3}}$. The first Brillouin zone of the reciprocal lattice is hexagonal (see Figure 1.5) and consists of four inequivalent high symmetry points which are Γ (in the center), M (in the center of the edge), K and K' (in the corners). These high symmetry points play an important role in the electronic properties of carbon nanotubes, discussed in the next section. [29]

1.2.2 Electronic Properties of Carbon Nanotubes

Carbon nanotubes can be represented as rolled graphene sheet, so one way to determine the electronic properties of CNTs is to use the graphene lattice as the base. Carbon has four valence orbitals (the $2s$, $2p_x$, $2p_y$ and $2p_z$ orbitals) from which three orbitals ($2s$, $2p_x$, $2p_y$) combine to form three hybrid sp^2 orbitals which have bonding σ and antibonding σ^* states. The bonding σ orbitals correspond to the strong covalent single bonds between the carbon atoms forming the hexagonal carbon lattice and they are responsible for most of the mechanical properties of the graphene sheet. The gap between σ and σ^* states is so large that they are not playing an important role in the electronic properties of graphene. In contrast,

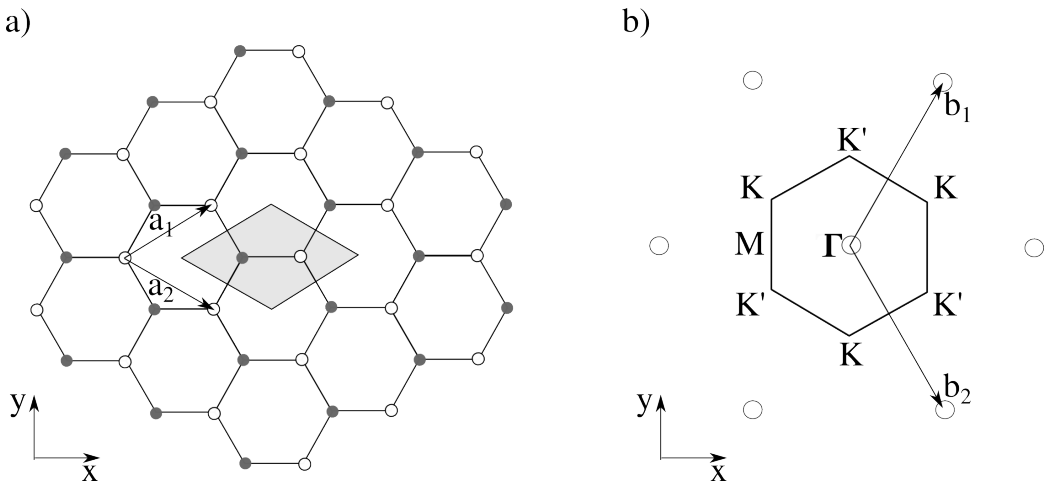

Figure 1.5: a) Graphene lattice with unit vectors ($\mathbf{a}_1$ and $\mathbf{a}_2$) and two inequivalent carbon atoms (white and gray dots). Gray area is the unit cell of graphene. b) The reciprocal space of graphene with the first Brillouin zone and reciprocal lattice vectors ($\mathbf{b}_1$ and $\mathbf{b}_2$). Γ, K, K′ and M represent the high symmetry points of graphene. Adapted from ref. [29].

the remaining p_z orbital that points out of the graphene sheet cannot couple with the σ states, but it can interact with neighboring p_z orbitals creating delocalized π (bonding) and π^* (antibonding) orbitals. These π bonds cause weak interactions between CNTs in a bundle and also weak interactions between carbon layers in graphite.

The bonding π (last valence) band and antibonding π^* (first conduction) band lie in the vicinity of the Fermi level E_f determining the electronic properties of the graphene and CNTs. A simple tight-binding model for these two π bands of graphene gives the dispersion relation, in other words, the energy dependence of the electronic motion:

$$E^{\pm}(k_x, k_y) = \pm\gamma_0 \sqrt{1 + 4\cos\frac{\sqrt{3}k_x a}{2}\cos\frac{k_y a}{2} + 4\cos^2\frac{k_y a}{2}}. \qquad (1.9)$$

where γ_0 is the transfer integral between first-neighbor π orbital and a is the lattice constant of graphene. The electronic momentum vector $\mathbf{k} = (k_x + k_y)$ belongs to the first hexagonal Brillouin zone and forms an ensemble of available electronic momenta shown in Figure 1.6.

This dispersion relation of graphene can be adapted for nanotubes by requiring the wave functions in nanotubes to satisfy the boundary conditions around the tube circumference. This is called an electronic zone-

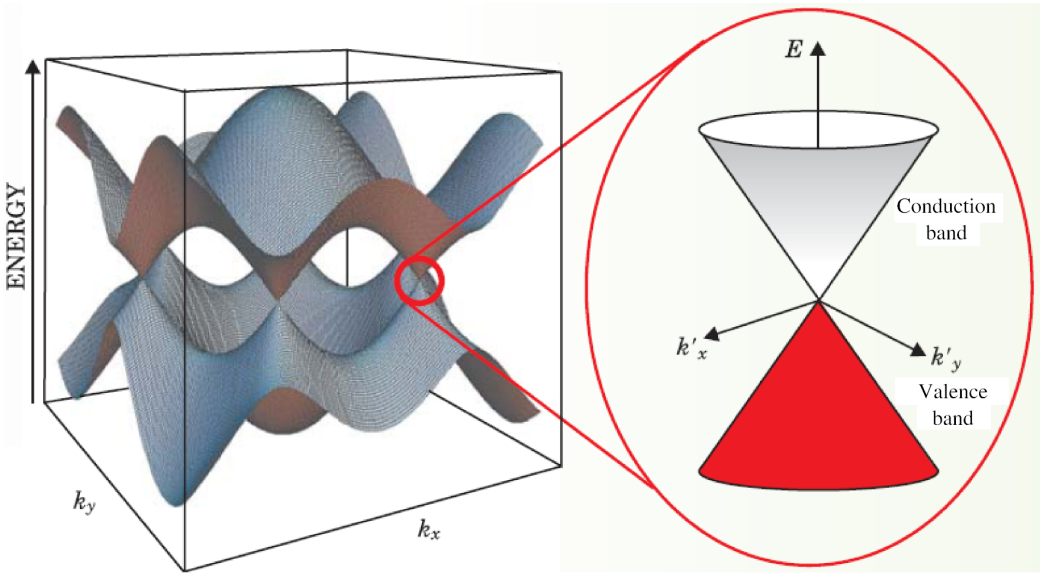

Figure 1.6: Dispersion relation describes the band structure of graphene. Graphene is called a semimetal or a zero bandgap semiconductor, because its valence (lower part) and conduction (upper part) bands touch at K and K′ points in the Brillouin zone (see the zoomed dispersion cone on the right). Adapted from ref. [30].

folding approximation, in which the periodic boundary conditions cause the quantization of the wave vectors around the nanotube circumference ($k_\perp$). The wave vectors along the nanotube axis ($k_\parallel$) are continuous for infinite tubes. When these allowed vectors for a certain nanotube are plotted onto the Brillouin zone of graphene (as in Figure 1.7), there forms a series of parallel lines whose length, number and orientation depend on the chiral indices (n, m) of the nanotube. The electronic band structure of a certain nanotube is given by superposition of the graphene electronic energy bands along the corresponding allowed $\mathbf{k}$ lines.

A closer look to this phenomenon leads on to the classification of carbon nanotubes to metallic and semiconducting tubes. When rolling the graphene sheet to a nanotube form, the periodic boundary conditions around the tube circumferential direction cause limitations on the allowed wave function quantum phase and quantize the wave vectors:

$$\Psi_{\mathbf{k}}(\mathbf{r} + \mathbf{C}_h) = e^{i\mathbf{k}\cdot\mathbf{C}_h}\Psi_{\mathbf{k}}(\mathbf{r}) = \Psi_{\mathbf{k}}(\mathbf{r}), \tag{1.10}$$

where the vectors $\mathbf{r}$ and $\mathbf{k}$ are taken on the surface of nanotube. This relation leads, depending on the chiral vector $\mathbf{C}_h = (n, m)$, to two possible

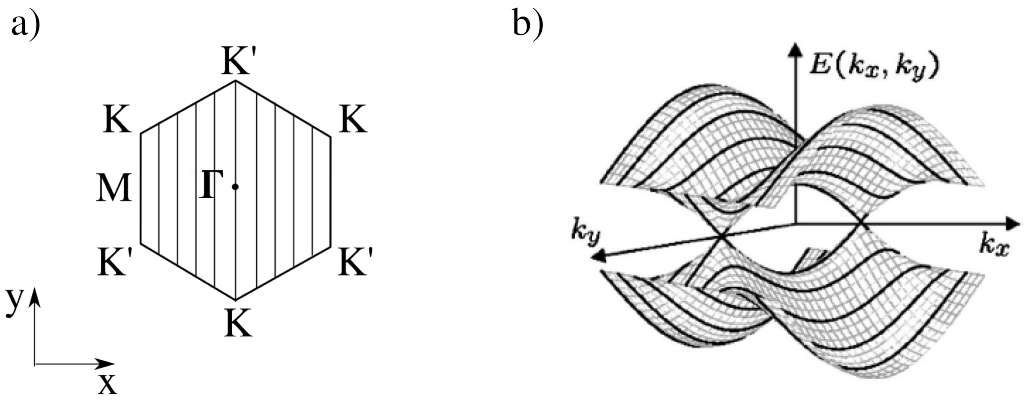

Figure 1.7: a) Brillouin zone of graphene. Parallel lines describe the allowed **k** vectors for the (5,5) armchair nanotube. b) Dispersion relation for graphene with dispersion relation of an (5,5) armchair nanotube (bold lines). In this case, the lines pass through the K and K' points, so the tube is metallic. If the lines are not going through the K and K' points, there will be an energy gap between the valence and conduction bands, and the tube is semiconducting. Adapted from ref. [22].

situations, when making an analysis near the Fermi surface (in other words, near the K points). Now $\mathbf{k}$ is $\mathbf{k} = \mathbf{K} + \delta\mathbf{k}$, where $\mathbf{K} = (0, 4\pi/3a)$ and $\delta\mathbf{k}$ small. When $n - m = 3l$ (l is an integer), the periodic boundary conditions produce $\delta\mathbf{k} \cdot \mathbf{C}_h = 2\pi q$ (q is integer). Each q value corresponds to a line of allowed $\mathbf{k}$ vectors generating a set of parallel lines through the Brillouin zone of graphene . When $n - m = 3l$, one k-line crosses the K point and the tube is metallic (see Figure 1.7). The dispersion relation for the metallic tube close to Fermi level is

$$E^{\pm}(\delta\mathbf{k}) \approx \pm\frac{\sqrt{3}a}{2}\gamma_0 \left\|\delta\mathbf{k}\right\|. \tag{1.11}$$

For the second situation, $n - m = 3l \pm 1$, the same analysis gives the dispersion relation near the Fermi level

$$E_q^{\pm}(k_{\|}) \approx \pm\frac{\sqrt{3}}{2}\gamma_0\sqrt{\left(\frac{2\pi}{|\mathbf{C}_h|}\right)^2\left(q \pm \frac{1}{3}\right)^2 + k_{\|}^2}, \tag{1.12}$$

where q is integer counting the available bands, and $k_{\|}$ is the vector component parellel to the tube axis describing the states within a given subband. This kind of nanotube having $n - m = 3l \pm 1$ is semiconducting, because the k-lines don't cross the K point. This causes an energy gap at

the Fermi level. The width of the energy gap can be calculated from the Equation 1.12:

$$\Delta E_g = E_c - E_v = E^+_{q=0}(k_\parallel = 0) - E^-_{q=0}(k_\parallel = 0) = \frac{2\pi a \gamma_0}{\sqrt{3}\,|\mathbf{C}_h|}. \qquad (1.13)$$

E_c is the energy on the edge of conduction band, and E_v is the energy on the edge of valence band respectively. The diameter of the tube is $d_t = |\mathbf{C}_h| / \pi$, so the gap size is inversely proportional to the tube diameter. In reality, the band gap depends on the chirality as well [31].

From these two chirality conditions (metallic: $n - m = 3l$, semiconducting: $n - m = 3l \pm 1$) it can be estimated roughly that $1/3$ of the tubes are metallic and $2/3$ are semiconducting. These calculations do not take into account that carbon nanotube has slightly different properties arising from curvature, such as slightly different C-C bond lengths perpendicular and parallel to the axis, and the effects of curvature to the hybridization and formation of σ and π bonds. Due to these differences, only armchair tubes are purely metallic tubes while other tubes with $n - m = 3l$ are small-gap semiconductors. For most practical purposes, the original classification of nanotubes (metallic: $n - m = 3l$, and semiconducting: $n - m = 3l \pm 1$) is valid at room temperature.

The density of states (DOS) is defined as the number of available states ΔN per given energy interval ΔE. The shape of DOS depends strongly on the dimensionality of the object. The DOS of the 1D system contains spikes called Van Hove singularities, because the density of states diverges close to the band maxima and minima. Carbon nanotubes are one-dimensional systems, so their DOS has such a spiky behavior (see Figure 1.8). The density of states for semiconducting carbon nanotubes is

$$\rho(E) = \frac{2a}{\pi\gamma_0\,|\mathbf{C}_h|} \sum_{q=1}^{2n} \sum_{s=\pm} \frac{\left|E^s_q(k)\right|}{\sqrt{(E^s_q)^2(k) - \epsilon^2_{qs}}}, \qquad (1.14)$$

where E^s_q is the energy of the certain branch at given k-line and ϵ_{qs} is analytically derived energy position of the Van Hove singularities. Metallic nanotubes have no band gap and the DOS is constant at the Fermi energy [32]:

$$\rho(E_F) = 2\sqrt{3}a_c c / (\pi\gamma_0\,|\mathbf{C}_h|). \qquad (1.15)$$

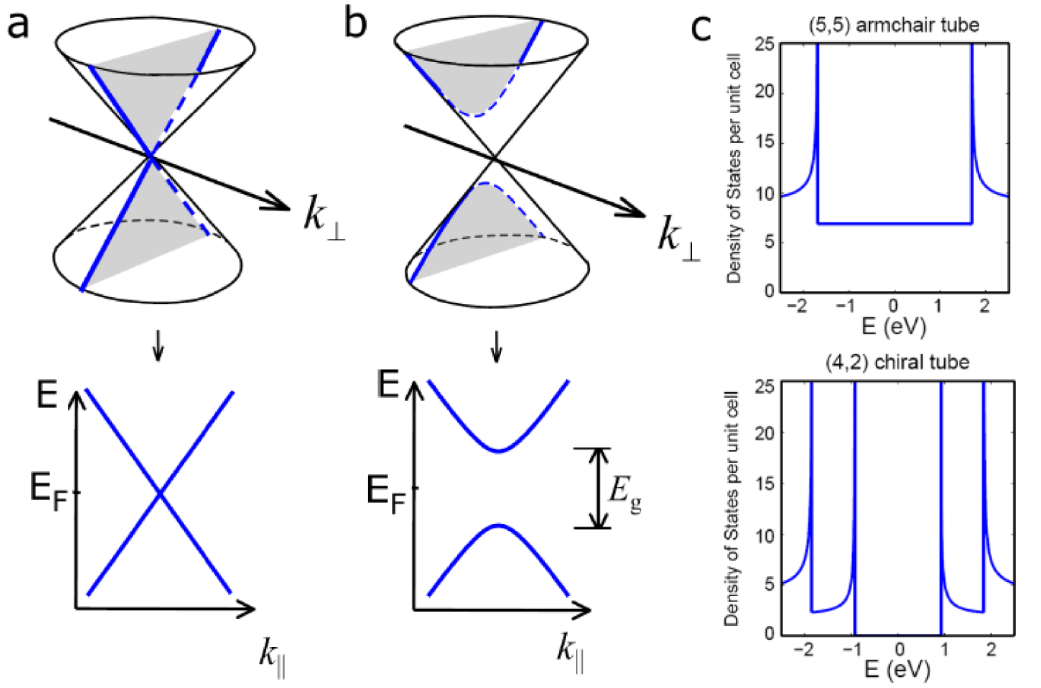

Figure 1.8: Schematic picture from the band gap formation near the dispersion cones. a) If allowed **k** lines go through the K points, there is no band gap, and the tube is metallic. b) If these lines bypass the K points, there forms a band gap E_g, and the tube is semiconducting. Note that the final electronic band structure of a certain nanotube is given by superposition of all allowed **k** lines. c) Density of states for a (5,5) metallic nanotube and a (4,2) semiconducting nanotube. The metallic nanotube has a finite DOS at the Fermi energy while it is zero for the semiconducting nanotube. Adapted from ref. [33].

1.2.3 Transport Properties of Carbon Nanotubes

The transport characteristics of carbon nanotubes can be derived from the Landauer-Buttiker formula which describes the conductance in 1D systems [34]:

$$G = \frac{Ne^2}{h}T. \tag{1.16}$$

where N is the number of transport channels, e is electron charge, h is Planck constant, and the variable T describes the transmission probability between the source and drain contacts. In the case of carbon nanotubes,

the number of transport channels N is four, because carbon nanotubes have two bands close to Fermi energy and both of the bands can transport one spin up and one spin down electron. The resistance is the inverse of the conductance, so the Equation 1.16 can be written as resistance $R = \frac{h}{4e^2} \cdot \frac{1}{T}$. The total resistance of carbon nanotube with metallic contacts can be written as [35]:

$$R(L) = \frac{h}{4e^2}(\frac{L}{l_m} + 1) + R_{nc}, \tag{1.17}$$

where L is the channel length, l_m is the electron mean free path and R_{nc} is the nontransparent contact resistance. For a device having a short channel length ($L << l_m$) and fully transparent contacts ($R_{nc} = 0$), the only resistance present is so called quantum resistance $R(L) = \frac{h}{4e^2} = R_Q = 6,45\,k\Omega$ and transport is said to be ballistic [36]. Metallic nanotubes have much higher l_m than semiconducting ones, and they have been shown to be ballistic even at room temperature [35].

The total capacitance of the nanotube consists of two different components:

$$\frac{1}{C} = \frac{1}{C_e} + \frac{1}{C_Q}, \tag{1.18}$$

where C_e is the electrostatic capacitance and C_Q quantum capacitance. C_e depends on dielectric structure and the geometry of the surroundings, and if the nanotube lies on a conducting substrate with a dielectric layer between them, the electrostatic capacitance is [37]

$$C_e \approx \frac{2\pi\epsilon\epsilon_0 L}{\ln(2t/d)}, \tag{1.19}$$

where ϵ is the average dielectric constant of the dielectric, t is the thickness of the dielectric, ϵ_0 is the dielecric permittivity, and L and d are the length and the diameter of the nanotube.

The quantum capacitance is [38]

$$C_Q = \frac{8e^2}{h\nu_F}, \tag{1.20}$$

where ν_F is previously defined Fermi velocity. Equation 1.18 shows that the smaller one of C_Q and C_e is dominant.

The inductance of carbon nanotube is a sum of quantum and classical inductances. The quantum inductance, usually called kinetic inductance,

is the resistance to change of the kinetic energy of the electrons and it is proportional to the density of states, whereas the classical inductance depends on the nanotube diameter, the geometry of the structure, and the magnetic permeability of the medium. The quantum inductance is in most cases the larger one, so it dominates the total inductance of the nanotube. [39]

1.3 Carbon Nanotube Field-Effect Transistor

Transistors play a crucial role in computers, phones and other modern technology applications based on integrated circuits. The performance of conventional silicon transistors is reaching its pysical limits in near future and cannot maintain a trend known as Moore's law (a doubling of the number of transistors on a processor chip every two years) [40]. Carbon nanotubes are among the most promising materials for future semiconductor technology [41] and they have potential to replace silicon in the transistors. In addition to small dimensions, carbon nanotubes have an extraordinary charge carrier mobility [42], tolerance to high current densities [43], and easy integration of different gate dielectrics into nanotube [44], which all make them a promising channel material for transistors.

This section describes shortly the principles of a conventional metal-oxide-semiconductor field-effect transistor, how it resembles the carbon nanotube field-effect transistors (CNT FETs), how Schottky barrier CNT FET works, and finally something about CNT FETs in sensor applications.

1.3.1 Conventional Metal-Oxide-Semiconductor Field-Effect Transistor

A metal-oxide-semiconductor field-effect transistor (MOSFET) has three terminals (electrodes) called source (S), drain (D), and gate (G). An electric field established between the gate and substrate is used to modulate the current from the source to the drain. A thin layer of SiO_2 is used as an insulator between the gate and the channel. The n-channel enhancement-mode MOSFET (in Figure 1.9) is one type of MOSFET providing the highest performance. There is no channel in this type of device; a conducting channel is induced by an electric field created between the gate and the p-type substrate. When a device or a material is said to be n-type, charge

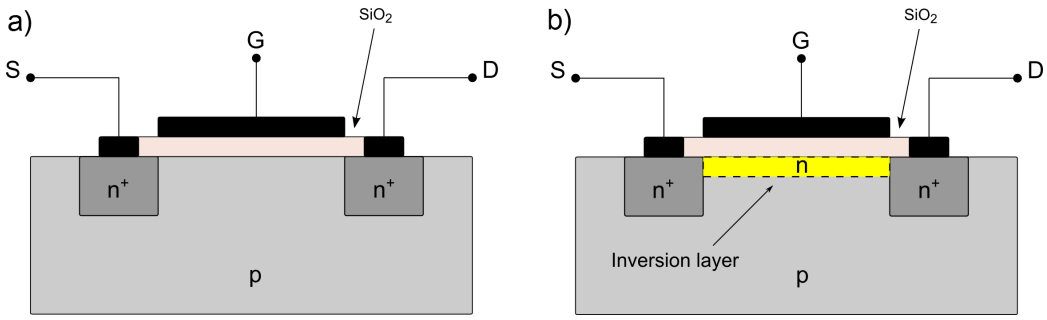

Figure 1.9: A schematic cross section of an n-channel enhancement-mode MOSFET. a) When the gate voltage is zero, only a small current can flow through the two back-to-back pn-junctions. b) When a positive voltage is applied to the gate, electrons are pulled from the p-type substrate towards the gate. An n-type layer of mobile electrons, called an inversion layer, forms near the surface of the semiconductor and the current can go through this channel from the source to the drain. Adapted from ref. [45].

carriers are electrons with a negative charge. Respectively, p-type devices or materials have positive charge carriers called holes, which are the vacanciens left behind to the lattice of the semiconductor by the electrons. When the gate voltage V_g is zero, small current flows through the two back-to-back pn junctions. With a small positive gate voltage, holes in the p material below the gate are repelled and a depletion layer forms on to the interface of the p material and SiO_2. The current is even smaller in this case. In a doped semiconductor the density of mobile electrons n and the density of holes p depend on the intrinsic carrier density n_i^2

$$np = n_i^2. \tag{1.21}$$

When adding more positive voltage, the density of holes is driven down at the interface of the p-type material that turns to n-type due to the fact in Equation 1.21. The formed n-type layer of mobile electrons is called an inversion layer and the current can go through this channel from the source to the drain. When the gate voltage becomes bigger than the so called threshold voltage (V_T), the transistor has been turned on, and the current can easily flow along a continuous n-type channel from the drain to the source (see Figure 1.9) [45].

The output characteristics of an n-MOSFET shows two different types of regions (see Figure 1.10): ohmic and saturation regions. For small positive drain-source voltages (V_{DS}) the current flowing through the transistor is

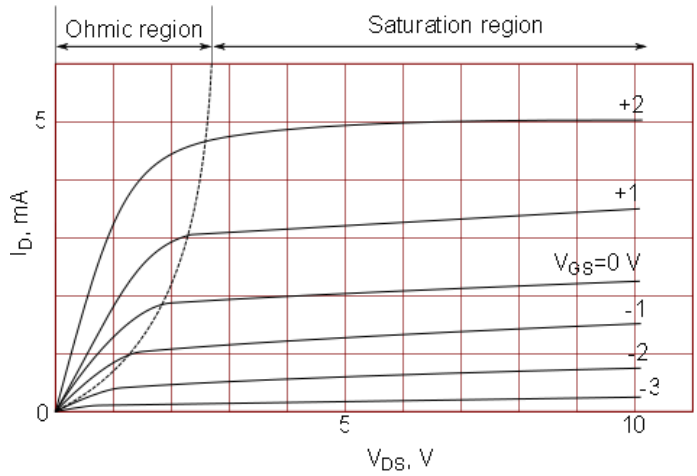

Figure 1.10: Typical I-V characteristics of n-channel enhancement-mode MOSFET. Adapted from ref. [45].

dependent on the magnitude of V_{DS} and has a resistance characteristic. This region is called the ohmic region. When V_{DS} is increased, the potential difference between the gate and the drain electrodes is decreasing and the amount of inversion charges decrease also on the drain side of the channel and the channel is in pinch-off. Due to this, the current increases much more slowly depending mainly on V_G. Thus, this region is called the saturation region [46].

1.3.2 Schottky Barrier at the Metal/Carbon Nanotube Interface

The first single-wall carbon nanotube field-effect transistor (SWCNT FET) was made in 1998 by Tans et al. [47] and soon after that Martel et al. demonstrated a field effect transistor based on a multi-wall carbon nanotube (MWCNT FET) [37]. In this thesis, the word "CNT FET" refers to SWCNT FET unless otherwise noted. A structure of a typical CNT FET (called also "device" in this thesis) is shown in Figure 1.11. A semiconducting CNT is contacted to metallic source and drain electrodes, and they lay on a highly doped silicon wafer. A thin, thermally grown silicon oxide insulates the nanotube and the silicon wafer that acts as a back gate. One essential similarity between an CNT FET and a MOSFET is the current

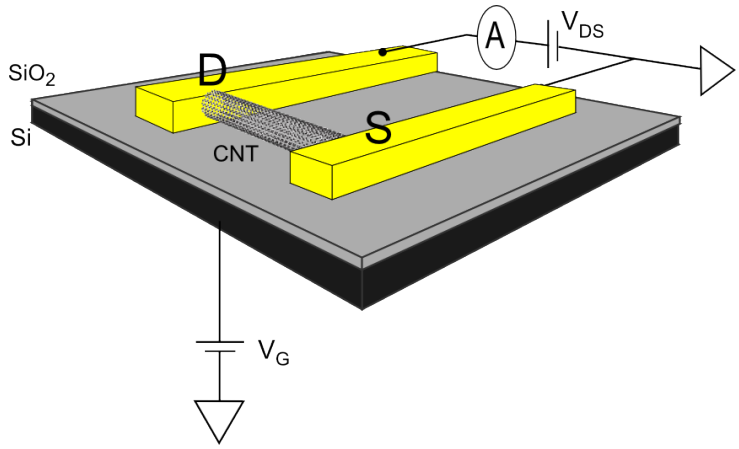

Figure 1.11: A schematic of a typical CNT FET together with a simplified measurement setup. A semiconducting CNT is contacted to metallic source (S) and drain (D) electrodes. The current between the electrodes through the nanotube is modulated with the gate voltage connected to a highly doped silicon wafer that is insulated from the electrodes and the tube by a thermally grown silicon oxide layer.

modulation: The current between the source and the drain electrodes through the nanotube channel is controlled by a third gate electrode. The MOSFET needs gate voltage to create the channel, but here in CNT FET the channel is already there.

There can exist two types of barriers for charge carriers between the metal electrodes and the carbon nanotubes which increase the conctact resistance to be beyond the ideal $R_q = h/4e^2$ limit (see secion 1.2.3). An imperfect interface between the metal and the nanotube creates one barrier, but a more fundamental issue is the Schottky barrier that affects many essential properties of the CNT FET, such as its contact resistance, on/off ratio, and subthreshold slope. Therefore it is important to understand how Schottky barriers form in CNT-metal contacts, and which factors affect their heights. [36]

According to the Schottky-Mott theory, the height of the Schottky barrier between a metal and a semiconductor is [48]

$$\phi_{SB} = \phi_M - \chi, \tag{1.22}$$

where ϕ_M is the work function for the metal, in other words, the energy required to move an electron from the Fermi level in the metal to the vacuum level. The vacuum level means the energy level where an electron

in the vacuum is so far from the metal that the electrostatic image force on the electron can be neglected [49]. The electron affinity χ is the energy difference between the bottom of the conduction band in the semiconductor and the vacuum level [50].

In reality, the dependence of the height of the Schottky barrier on the work function of the metal is much weaker in traditional semiconductor-metal contacts. This is caused by a phenomenon called Fermi level pinning that has been highly controversial producing a variety of models. [51]

The metal induced gap states (MIGS) model [52] is probably the most popular among these models. When a bulk metal is brought into close contact with a bulk semiconductor, the Fermi level of the metal and the charge neutrality level of the semiconductor (the energy where the gap states cross over from valence- to conduction-type character [53]) align and thermodynamic equilibrium is reached in the system. This alignment happens through the transfer of electrons from the conduction band of the semiconductor into the metal or vice versa, depending on the relations between the work functions. As a result of this charge transfer, a dipole layer is formed at the metal–semiconductor interface creating MIGS to the semiconductor side of the interface. The dipole shifts the bands inside the semiconductor, and near the interface the bands of the semiconductor bend and decay exponentially into the semiconductor. As a result the barrier near the interface is either raised or lowered [50, 54]. Thus the height of the formed Schottky barrier is nearly independent of metal work function [52]. The barrier height for electrons is then approximately

$$\phi_{SB}^{n} \approx E_C - E_N, \tag{1.23}$$

where E_C is the energy of the bottom of the conduction band in the semiconductor and E_N is the charge neutrality level of the semiconductor. In the case of semiconducting CNTs, the band structure of the CNT is exactly symmetric (see the π-orbital model described in the section 1.2.2), thus the charge neutrality level will be at the middle of the band gap E_g. [55]

The formation of the Schottky barrier depends strongly on the geometry of the contact, so a 2D planar contact between bulk materials is not similar to a contact between a bulk metal and a 1D nanotube. The properties of the contact are also different between side contacted (weak van der Waals forces) and end bonded (strong covalent/metallic bonds) nanotubes (see Figure 1.12) [56]. For the planar junction between a bulk

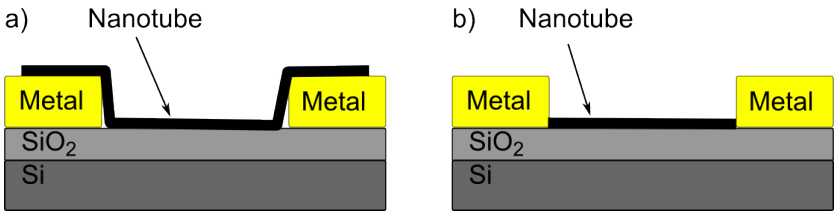

Figure 1.12: The type of the contact between nanotube and metal affects the properties of the contact. a) Nanotube side contacted by the metals by weak van der Waals adhesion. b) Nanotube end bonded to the metals by covalent/metallic bonds. Adapted from ref. [55].

metal and the semiconductor, the dipole is a 2D sheet which shifts the semiconductor bands relative to the metal Fermi level even at distances comparable to the lateral dimensions. In contrast, the small contact area between the metal electrode and the end bonded nanotube causes the localization of the dipole in all three directions, so the effect of the dipole decays as d^{-2} at distances greater than 2 nm. Thus the bands of the nanotube bend only locally near the surface, and inside the nanotube they stay intact (see Figure 1.13). Therefore the height of the Schottky barrier is determined only by the work function of the metal, and it can be controlled by choosing an appropriate metal. [55]

In the case of side contacted nanotube the role of Fermi level pinning is still unclear [53]. There are only weak van der Waals forces between the metal and the nanotube [55], so interaction between the two materials is weak leading to high contact resistances. When approximating this interaction to zero, interface states do not form (see fig 1.13), in which case a p-type Schottky barrier for hole injection between metal fermi level and valence band of nanotube is [57]:

$$\phi_{SB}^{p} = \phi_{NT} + \frac{1}{2}E_g - \phi_M, \tag{1.24}$$

where ϕ_{NT} is a work function of the nanotube. Respectively, an n-type Schottky barrier for electron injection between metal fermi level and conduction band of nanotube is [57]:

$$\phi_{SB}^{n} = \phi_M - \phi_{NT} + \frac{1}{2}E_g. \tag{1.25}$$

As mentioned earlier, the charge neutrality level will be at the middle of the band gap and thus the work function for an intrinsic carbon nanotube is defined as $\phi_{NT} = \chi + \frac{1}{2}E_g$ [58]. In some cases, doping (tuning the

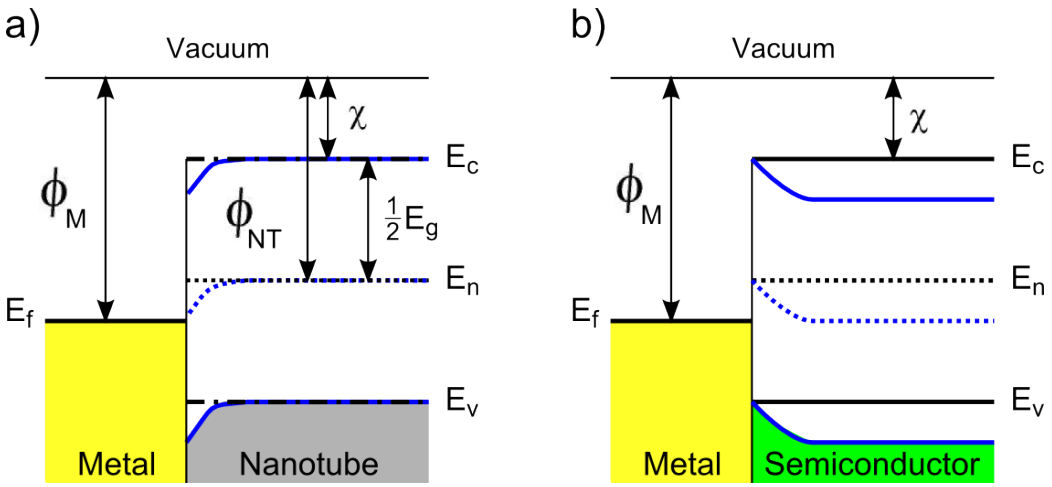

Figure 1.13: Differences in Schottky barrier formation between metal/nanotube and metal/bulk semiconductor. a) The case for contacts between the metal and the nanotube, when there is no interface dipole (black lines, the extreme case of the side contacted nanotube) and with strong interface dipole (blue lines, end-bonded nanotube). b) The contact between bulk metal and bulk semiconductor. Black lines represent the situation before contact. After contact, bands bend near the interface (blue lines). Note that in addition to bending, the bands inside the bulk semiconductor shift downwards.

electronic properties of the nanotube) is supposed to shift the bands of the nanotube [3, 59–61], so the charge neutrality level is no more in the middle of the band gap. The effects of doping on the Schottky barrier are discussed later in section 4.3.7.

The band gap of the CNT along with the work function of the metal determine what kind of contact will form. When the metal and the nanotube are contacted, the Fermi level of the metal and the charge neutrality level of the nanotube align at the interface. The work function of CNT is reported to be 4,7-4,9 eV [62], so the contact between a CNT and a high work function metal, such as palladium (ϕ_{Pd}=5,1 eV [63]), forms usually a p-type contact, as in Figure 1.14a. Respectively, the CNT contacted with a low work function metal like scandium (ϕ_{Sc}= 3,3 eV [63]) has more n-type behavior, as in Figure 1.14b. If the work function of the metal is outside the band gap of the nanotube, there is virtually no potential barrier between the metal and the semiconductor (zero or slightly negative Schottky barrier), and the charge carriers can flow freely through the contact. This is called ohmic contact and it has been successfully formed between palladium and a carbon nanotube with a diameter $\approx$ 1,6

nm [36].

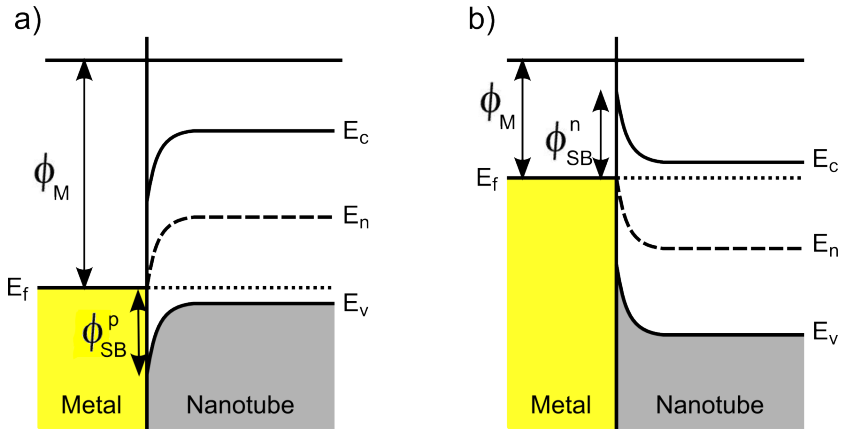

Figure 1.14: The effect of the metal work function on the formation of the schottky barrier. a) A nanotube end bonded with high work function metal. With small negative gate voltage, the bands inside the nanotube shift upwards enough to enable holes to tunnel through the Schottky barrier. Respectively, electron tunneling through the interface needs high positive gate voltages, thus the contact is more p-type. c) A nanotube end bonded with low work function metal. Now the barrier for electrons is lower, so the contact is more n-type. Adapted from ref. [57].

The wetting properties of the metal (how well the metal covers the surface of the nanotube) also have a big role in the behavior of the junction. If the metal wets well (e.g. palladium), it takes the form of the nanotube surface giving a large contact area between them. With low wetting (e.g. platinum), the metal is in clusters on the surface and the contact is poorer. This explains the different performances of the CNT FETs with metal electrodes having similar work functions such as palladium and platinum. [36]

The charge carrier transport through the metal/nanotube interface can happen by thermally assisted tunneling through the Schottky barrier or by thermionic emission over the Schottky barrier. Tunneling is usually the dominating factor, so when the thickness of the barrier depends on the external electric fields, the gate voltage can be used to modulate the current through the barrier [64, 65]. Figure 1.15 shows a simplified transport characteristics of CNT FET and snapshots of the Schottky barrier near the source contact with six different gate voltages. The work function of the metal lies in the band gap of the nanotube and a strong interface dipole is formed on the contact. As it can be seen, the gate voltage shifts the

energy bands inside the nanotube affecting the carrier transport through the barrier. When V_g is zero (point d in the figure 1.15), the Fermi level of the metal and the charge neutrality level of the nanotube are aligned and there is only a small current through the device due to thermally assisted tunneling through the Schottky barrier to the valence band of the nanotube. Small negative V_g shifts the bands upwards and reduces the width of the Schottky barrier enabling higher hole currents through it to the valence band of the nanotube. When the bands inside the nanotube are shifted upwards enough, valence band aligns with the Fermi level of the metal (c), and a charge starts to accumulate in the nanotube. The gate voltage in this situation is called the threshold voltage V_{TH}. When increasing the negative V_g, the band shifting inside the nanotube starts to slow down (b) decreasing the thinning of the Schottky barrier. After this point the bands are not shifting anymore (a) and the current I_d saturates to constant value. Respectively, for positive V_g the bands shift down and become flat in point (e), where the current is at its minimum. When positive gate voltage is increased, the bands shift down enough enabling electrons to tunnel through a Schottky barrier between the metal Fermi level and the conduction band of the nanotube (f). This example has both p-type (holes as carriers) and n-type (electrons as carriers) behaviors, so it is slightly ambipolar CNT FET. Respectively, if the device exhibit only one type of behavior, it is called unipolar [66].

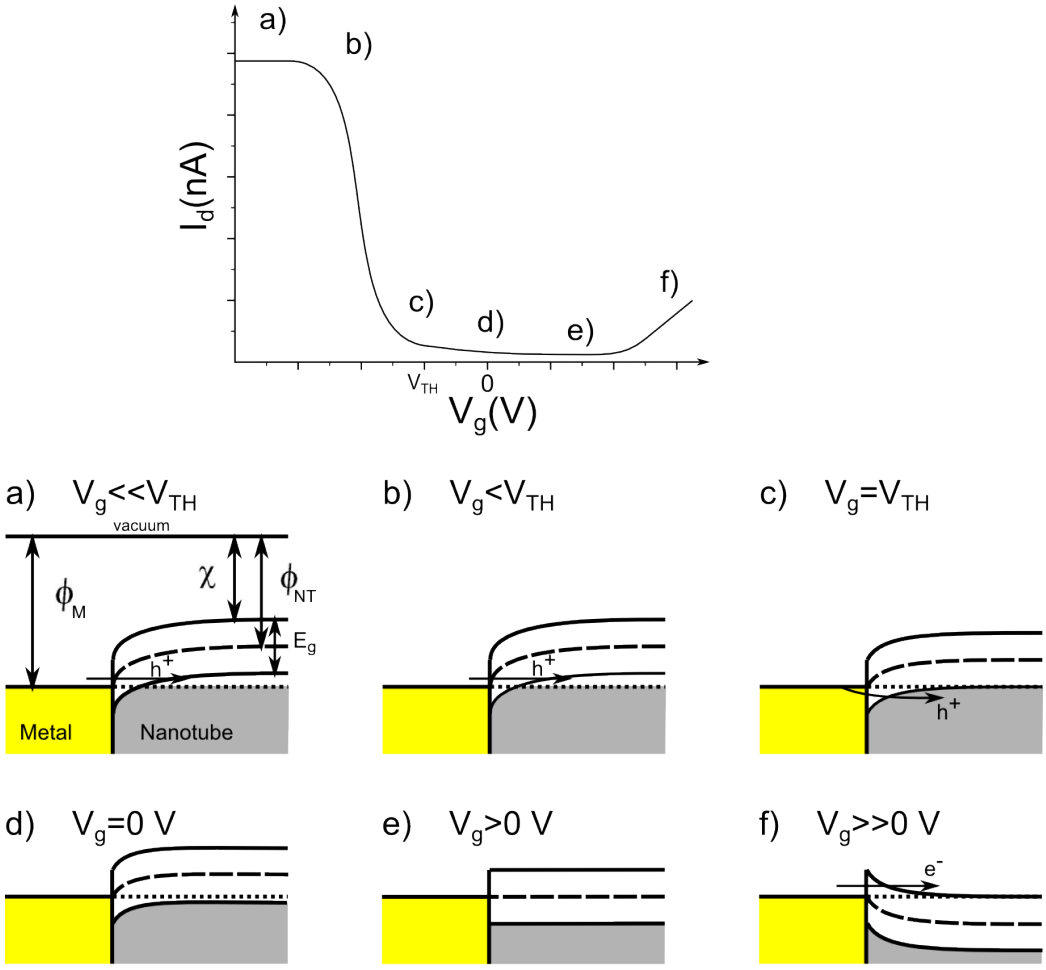

Figure 1.15: Operation principle of a CNT FET. A simplified transport characteristics of CNT FET (drain current I_d versus gate voltage V_g) with fixed drain-source voltage V_{ds} sketched on top. The snapshots of the Schottky barrier near the source contact are shown with six different gate voltages (from a to f). Adapted from ref. [67].

1.3.3 Main Characteristics of CNT FET

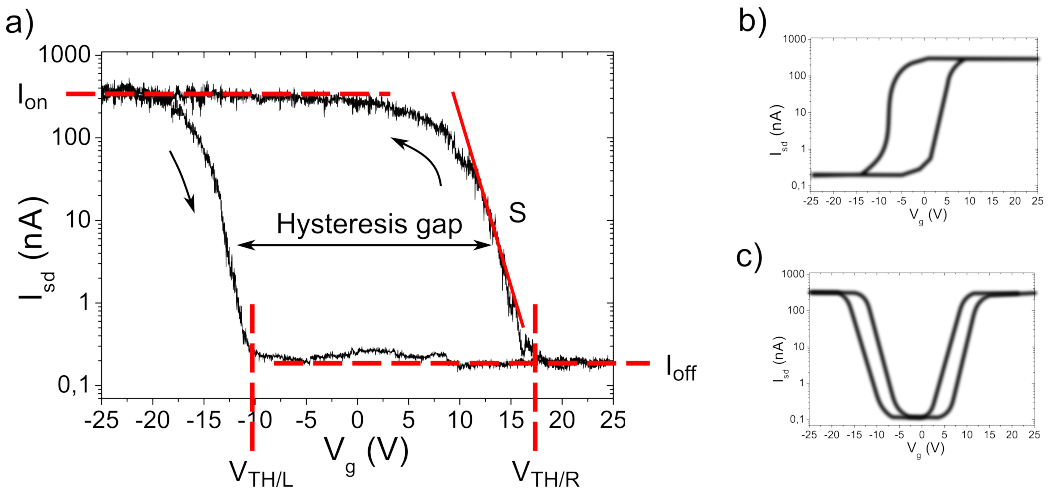

Figure 1.16: a) Typical transfer characteristic of p-type CNT FET. I_{on} and I_{off} are ON and OFF state currents, $V_{TH/L}$ and $V_{TH/R}$ are left and right threshold voltages, and S is subthreshold slope. The hysteresis is counter clockwise in this case, and its size is $V_{th/r} - V_{th/l}$. In addition, rough schematics of transfer characteristics of n-type CNT FET in b) and ambipolar CNT FET in c).

Figure 1.16a shows a typical transfer characteristic of a p-type CNT FET, in other words, a source-drain current I_{sd} versus gate voltage V_g for a constant source-drain voltage V_{ds}. A few important parameters (threshold voltages, ON/OFF ratio, subthreshold slope, and hysteresis) describing the performance of a transistor, are marked on that Figure. Figures 1.16b and 1.16c show rough schematics of transfer characteristics of n-type CNT FET and ampibolar CNT FET, respectively. Generally speaking, p-type CNT FET is ON with negative gate voltages and OFF with positive gate voltages. N-type CNT FET works vice versa being ON with positive gate voltages and OFF with negative gate voltages. Ambipolar CNT FET is OFF with small gate voltages and reaches its ON state with higher (both positive and negative) voltages.

The ratio between ON state current I_{on} and OFF state current I_{off} is called the ON/OFF ratio, and it gives information about how well the transistor closes. It is important to maintain low leakage current to keep both the passive power at a minimum and a sensible ON/OFF ratio (above 10^4 is usually needed for logic applications). Unipolar CNT FETs have these ratios in the range of 10^5–10^7. [68]

Another important parameter is the inverse subthreshold slope [68]

$$S = (d \log_{10} I / dV_g)^{-1} \tag{1.26}$$

that describes how efficiently the gate voltage switches the channel. In a transistor with ohmic source and drain contacts (such as conventional Si MOSFET), S is limited by thermionic emission over the channel and it is about 60 meV per decade at 300 K. When Schottky barrier dominates the transport in a transistor, S is significantly higher, about 100-150 mV per decade for oxide thickness smaller than 10 nm. A few studies have succeeded to decrease S by tuning the Schottky barriers at the contacts. A subthreshold slope of 60 mV per decade has been achieved by a double-gated CNT FET [66] and around 40 mV per decade by a CNT FET taking advantage of band-to-band tunneling [69].

The threshold voltage is the value of the gate voltage, in which the CNT FET starts to conduct. In this case, there are two different threshold voltages, $V_{th/l}$ and $V_{th/r}$, due to the shift between forward and reverse gate bias sweeps called hysteresis. The short arrows show the directions of the gate bias sweeps in the Figure 1.16 indicating that the hysteresis is counter clockwise. The size of the hysteresis gap is $V_{th/r} - V_{th/l}$.

Hysteresis is a very common phenomenon in CNT FETs. This phenomenon can restrict the possibilities to use them for electronic integrated circuits, so its origin has been tried to resolve quite intensively. There are several different theories for that, but the screening effect caused by the charge exchange between CNTs and their surroundings is commonly believed to be the main reason for hysteresis [70]. The hysteresis can be controlled [71] or even removed [72] by modifying the surroundings of the nanotube.

One widely quoted explanation for the hysteresis is the surface-bound water layer which works as a charge trap or mediator [73], but its reliability has been questioned [74]. A popular insulator between the nanotube and the back gate is thermally grown silicon oxide that was used in the experiments of this thesis, too. One theory proposes that the silanol groups (≡SiOH) on the silicon oxide surface act as the charge traps or sources [75] and there forms a net positive charge near the tube that adds to the gate potential causing a negative shift to the G–V_g curve.

Another recent study supports also the fact that the charge injection around the nanotube is responsible for the hysteretic behavior of CNT FETs [76]. According to that study, the adsorbed water layer on the SiO_2 surface is the main charge trap at room temperature, while other defects

influence more at high temperatures.

Hysteresis varied from moderate to wide in all of our devices, but it was not the main target in this study, so only forward gate sweeps are shown in the results.

1.3.4 CNT FETs as Sensors

A sensor is a device which measures a physical quantity, typically electronically, and converts it into a signal to be recorded elsewhere. The most important properties of sensors are selectivity, sensitivity and stability [77].

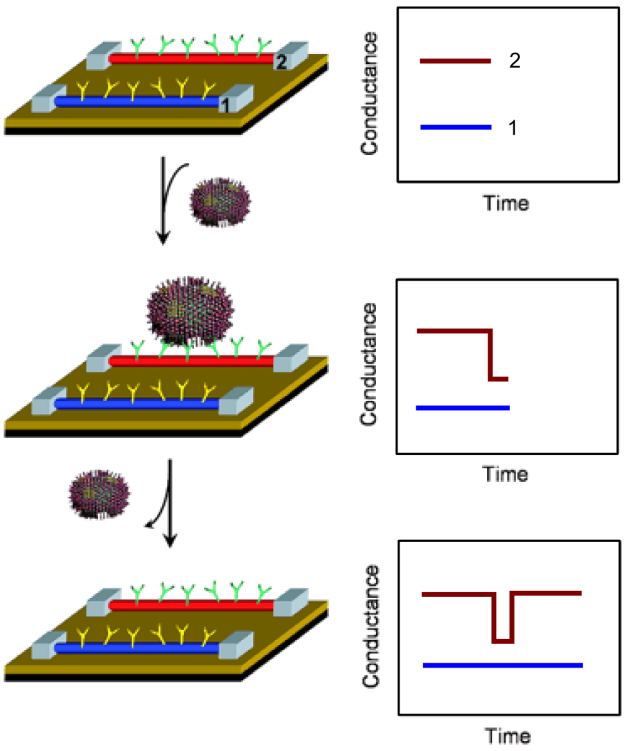

Figure 1.17: Schematic of nanowire (e.g. carbon nanotube) based detection of single viruses. Two devices, 1 and 2, are modified with different antibody receptors. When a single virus binds specifically to the receptors on nanowire 2, it produces a conductance change only in nanowire 2 which is a charasteristic of the surface charge of the virus (shown on right). When the virus unbinds from the surface of nanowire 2, the conductance returns back to the original. Adapted from ref. [78].

Carbon nanotubes are extremely attractive for fabricating sensors due to their outstanding properties highly suitable for sensor applications and

their potential for miniaturization and lower power consumption. Their reduced dimensions generate new interesting physical properties and they are composed entirely of surface atoms thus leading to a high environmental sensitivity. This property combined with excellent electronic properties of carbon nanotubes explain the ability of CNT FETs to detect very low amounts of the target analyte. [79]

CNT FET is a promising base structure for sensor applications, which offers a simple way to utilise the excellent electrical and chemical properties of CNTs. In addition, CNT FET can be potentially integrated to complex microelectronic systems with determined performance. CNT FETs have been used for sensing gas (NH_3, NO_2, H_2, CO, H_2S, etc.) or organic vapor molecules (e.g. ethanol and methanol). CNT FET based biosensors can detect various biological species such as DNA, proteins and cells. [79]

Functionalisation is adding or bonding something to the nanotube and it can be used to change their reactivity and thereby enhance their sensing performance. Functionalisation can be used to tune the electronic properties of nanotubes (called "doping", see Section 2.1) or to coat the nanotube to block unwanted reactivity [24]. Some gas sensor devices use functionalized nanotubes, because pristine carbon nanotubes can have a sensitivity too low to analytes due to low adsorption, low selectivity or a long recovery time [79]. For example, substitutional doping of impurity atoms into intrinsic CNT improves the adsorption of CO and water molecules on the tube [80].

The sensing mechanism of CNT FETs is still under debate due to very different conductance effects observed in sensing measurements. In addition, similar conductance variations have been interpreted differently. There are four proposals for possible sensing mechanisms of CNT FET biosensors: electrostatic gating [81–83], capacitance modulation [84], Schottky barrier effects [85–87], and carrier mobility change [88, 89]. According to a recent study, electrostatic gating and Schottky barrier effects seem to be two the most relevant mechanisms [90]. The sensing mechanisms of gas are slightly different from biosensing. For example, NH_3 detection bases on Schottky barrier for temperatures below 150 °C and charge transfer for higher temperatures [91]. The selective, spontaneous redox properties between Hg^{2+} and CNTs were proposed to be an explanation for the detection of mercuric ions in solution [92].

There are still many challenges to overcome before sensors based on carbon nanotubes can be exploited on a large scale. The commercial

production of pure and defect-free carbon nanotubes with the wanted properties (diameter, length, chirality) is difficult and expensive. The processing of nanotubes is still not fully controlled and all prepared single nanotube devices are individuals with somewhat different properties. In the field of biosensors non-specific adsorption of proteins to the walls of nanotubes are not prevented. In addition the health risks of carbon nanotubes are not known well, which limits their use especially in bioelectronics and with devices integrated with living biological systems. [24,77]

Despite some challenges of carbon nanotubes in sensor applications, the growing research interest in this field can offer answers for them. It is believed that carbon nanotubes will dramatically change the future of sensor industry.

Chapter 2

Previous Studies

2.1 Doping of Carbon Nanotubes

The delocalised electron system defines mainly the electronic properties of CNTs, so they are easily tuned by any chemical modification of the CNTs. By choosing properly the type of the modification, one can consciously tune the electronic properties of CNTs. This kind of tuning is typically called "doping". [93]

Many essential microelectronic components, such as rectifying p-n junctions, bipolar junctions, and field-effect transistors, are based on doped bulk semiconductors. Carbon nanotubes are potential key elements for future miniaturized electronics [94], so doping of carbon nanotubes can yield nanoscale devices with interesting properties and functions. Doping has been successfully used to enhance the field emission of MWCNTs [95], to improve Li ion affinity in the nanotubes for battery applications [96], to prepare better gas sensors [97], and to create active sites for the efficient covalent anchoring of molecules to the surface of MWCNTs [98].

Graphene is chemically inert due to its stable, planar, and aromatic sp^2-bonded carbon network. Only a few very reactive compounds can break this conjugated π-surface. In carbon nanotubes, the bending of the carbon network introduces strain causing curvature-induced pyramidalization of the single carbon atoms, and π-orbital misalignment between adjacent pairs of carbon atoms, which increase the chemical reactivity of carbon nanotubes slightly compared to graphene. Possible defects in the nanotube lattice also increase the reactivity. [93]

A remarkable difference between conventional 3D materials and 1D carbon nanotubes is that the material in the nanotubes is effectively all

surface. The unique structure of carbon nanotubes opens up many possibilities to dope them and change their physical and electronic properties not available in conventional 3D materials, such as chemical functionalization of the tube surface and π-stacking with aromatic or aromatic-containing molecules (see Figure 2.1). The discussion in this section presents shortly the main chemical modification techniques of carbon nanotubes focusing on the doping point of view. In addition, the transfer characteristics of CNT FETs can be tuned by modifying the interface between the nanotube and the contact electrode. This research field is shortly introduced at the end of this section.

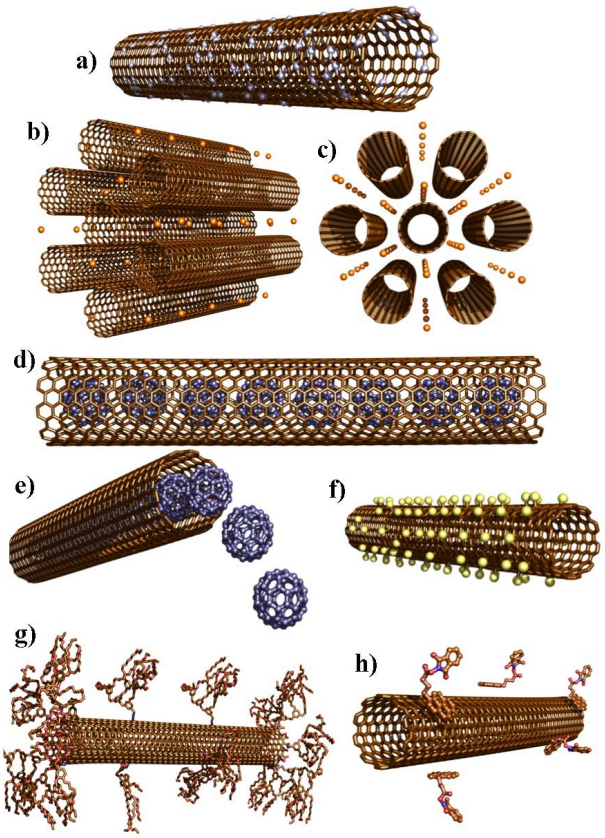

Figure 2.1: The unique structure of CNT provides many possibilities for its chemical modification. (a) substitutional doping of CNT, (b,c) nanotube bundles intercalated with atoms or ions, (d,e) CNTs filled with fullerenes, (F) fluorinated CNT, (g) covalent functionalization, (h) non-covalent functionalization via π-stacking. Adapted from ref. [93].

2.1.1 Substitutional Doping

One way to carry out substitutional doping is to introduce foreign atoms during synthesis of carbon nanotubes resulting in substitutional or interstitial impurities within the hexagonal lattice of carbon [99]. Substitutional doping can also be done by ion implantation [100].

Boron and nitrogen atoms are natural choices of dopants, as they have roughly the same atomic radius as carbon, while they have one electron less/more than carbon. When boron atoms substitute for carbon atoms within a carbon nanotube, there forms three-coordinated boron, and sharp localized states appear below the Fermi level due to the presence of holes in the structure. Thus boron causes p-type doping. From the chemical point of view, this structure reacts easier with donor-type molecules. [101]

Two kinds of C–N bonds can form in nitrogen doping. The first is a three-coodinated nitrogen which creates sharp localized states above the Fermi level. These states are caused by the presence of additional electrons and the tube can be considered as an n-type conductor. Chemically they react strongly with acceptor molecules. The second type of C–N bond has a two-coordinated nitrogen atom which can be connected to the hexagonal lattice of CNT, if an additional carbon atom is removed from the lattice. This induces localized states below and above the Fermi level and thus the doped tube is either a p- or an n-type conductor. [101]

In addition to tuned electrical properties, substitutional doping leads to a more reactive surface which is useful in many applications. It also induces defects and thereby lowers the mechanical strength of the nanotube, but this drawback can be minimized by using low doping concentrations. [101]

2.1.2 Intercalation

Bundled CNTs can be doped by electron-donating (e.g. alkali metals) or electron-accepting (e.g. halogens) small atoms or molecules that reside in the interstitial channels. Chemical doping increases the density of free charge carriers resulting in enhanced electrical and thermal conductivity in the bundles. When a CNT accepts electrons, the charge transfer weakens the C-C bonds in the tube [102] and downshifts certain Raman-active mode frequencies. Respectively, when CNT donates electrons, the C-C bonds stiffen causing upshifts in those mode frequencies. [101]

2.1.3 Endohedral Doping or Encapsulation

The capillarity of carbon nanotubes was first theoretically predicted by *Pederson* and *Broughton* [103]. Based on that prediction, researchers have tried and succeeded to encapsulate atoms, molecules, and crystalline materials inside nanotubes. Water transport inside carbon nanotubes raises great interests in biology and nanofluidics [101]. The water-filled cavity in the interior of nanotubes also opens up possibilities to perform chemical reactions there inside the nanotubes, thus leading to a unique nanoreactor [104]. Encapsulation of organic molecules is used to create hybrid systems with modified electronic and optical properties [105].

2.1.4 Non-Covalent Functionalization

Molecules or atoms can also be attached to the sidewall of a carbon nanotube. Non-covalent functionalization is an interesting method for doping carbon nanotubes because it is not disturbing the conjugated π-electron system of the carbon nanotube, and the intrinsic electronical and mechanical properties of the nanotubes are preserved. The interactions in non-covalent functionalization are primarily hydrophobic, van der Waals, and electrostatic forces. [106]

Aromatic molecules are known to interact with carbon nanotubes via $\pi - \pi$ interactions called $\pi - \pi$ stacking, and there can occur electron transfer between the nanotube and the absorbed aromatic molecule. Thus, aromatic molecules have been used to combine carbon nanotubes with different donor or acceptor units to investigate the photophysical properties of e.g. some supramolecular systems. [106]

Carbon nanotubes can be functionalized noncovalently with surfactants, polymers, and biopolymers (proteins, lipids, DNAs, etc.) which contain aromatic rings or other parts favorable for π-stacking [106]. The type of CNT FET has been shown to change from metallic behavior in dry conditions to semiconductor behavior in wet conditions after helical wrapping of DNA [107].

2.1.5 Covalent Functionalization

In a covalent functionalization, atoms or molecules are anchored covalently onto the sidewalls and open ends of carbon nanotubes [106]. Covalent functionalization has been shown to seriously modify the electronic struc-

ture of carbon nanotubes. It has also been used to separate bundled CNTs and to prepare stable solutions of CNTs in solvents [108]. The shift in the Raman spectra of functionalized carbon nanotubes shows evidence of charge transfer from the functional groups to the nanotube [109]. Fluorination and hydrogen functionalization have been proved to convert metallic carbon nanotubes to semiconducting ones [110].

Compared to air sensitive alkali-metal doping, the covalent functionalization provides a tool to produce more stable doped carbon nanotubes. However, there is one reason which limits the usage of covalent functionalization. The modification of the sp^2 carbon framework causes disorders on CNT sidewalls, which has effects on the inherent electrical and optical properties of the nanotubes [108]. For example, fluorination has been noticed to dramatically increase the resistance of CNTs [111].

2.1.6 Modifying Metal/Nanotube Contact

Tuning of the electronic properties of CNT FETs can be done without touching carbon nanotube itself. As discussed in Section 1.3.2, the properties of CNT FET depend highly on the metal/nanotube contacts. Thus one can tune the electronic properties of CNT FET by changing the contact metals or exposing the contact e.g. to oxygen [60, 61].

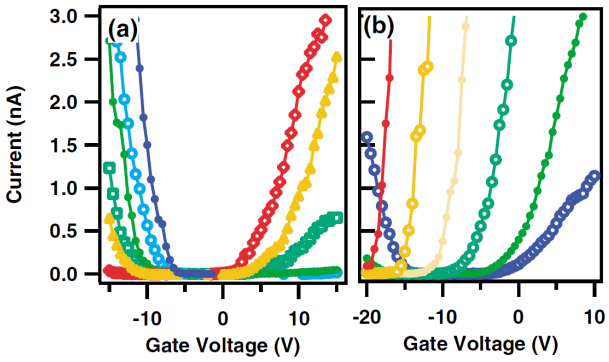

Figure 2.2: Experimentally measured transfer characteristics of CNT FETs during (a) oxygen adsorption and (b) potassium doping. In (a) n-type FET prepared by annealing in vacuum has been exposed to oxygen for 2 min per each stage at increasing pressures from 0 Torr to ambient in order: red, orange, light green, dark green, light blue and blue. In (b) the deposited amount of potassium increases from right to left (blue, dark and light green, light and dark orange, red). Adapted from ref. [60].

Metals with low work function, such as scandium [63] and yttrium [112], has been successfully used to fabricate high quality n-type CNT FETs. Similar results have been shown by coating CNT FETs with hafnium dioxide, HfO_2 [113].

2.2 Alkali Solution

In our previous studies [114], alkali solution was first used for separating bundled CNTs. Gas-phase alkali metals have been proved to dope carbon nanotubes [1,2]. In addition, some measurements done with alkali metals dissolved in solution hint that liquid-phase alkali metals also affect the electrical transport properties in some extent [4,5]. Based on these facts, it was reasonable to postulate that alkali solution can dope carbon nanotubes, which also was the main aim of this study.

2.2.1 Graphite Intercalation Compounds

The insertion of guest species between the layers of the graphite is possible due to the weak van der Waals interlayer forces in graphite. The formed product is called graphite intercalation compound (GIC). The guest species can be either atomic or molecular and there can be charge transfer between the intercalate and host layers. The free carrier concentration of the graphite host is very low at room temperature, thus intercalation with different species and concentrations allows wide tuning of the free carrier concentration and permits variation of the electrical, thermal, and magnetic properties of the host material. [115]

Alkali metals are common donor intercalants. GICs have many applications among which lithium based GICs are widely used in Li-ion secondary batteries for cell phones, personal computers etc. Carbon nanotubes can be used as a host material of GICs, too. In this case, the guest species are believed to decorate the exterior of the single wall carbon nanotubes, and they can also enter the hollow cores of the nanotubes (see Figure 2.1b,c). [115]

2.2.2 GICs for Separating Bundled Nanotubes

Single-wall carbon nanotubes exist typically as ropes or bundles of 10-30 nm in diameter due to their smooth surface and strong van der Waals

force between them [116]. Since clean, undamaged and individual CNTs are needed for many applications, a number of different separation methods have been developed, but many of them cause damage or cut the nanotubes to smaller pieces. In nanotube GICs, the intercalated species counterbalance the strong van der Waals energy between the nanotubes making the separation of the tubes easier. *Penicaud* et al. have developed a mild and effective separating method [117] based on this fact and demonstrated a polyelectrolyte salt of alkali metal and CNTs which can be dissolved in polar organic solvents spontaneously without sonication or other damaging methods. Final product is uncut, unmodified and well-separated CNTs in solution. The same process was repeated successfully with some modifications in our group producing solutions of individual CNTs [59, 114].

The alkali solution has to be prepared in an inert atmosphere due to high reactivity of alkali metals' with oxygen and humidity. At first, solid naphthalene is dissolved in polar aprotic solvent tetrahydrofuran (THF), and metallic lithium is added to this solution at room temperature. Refluxing is needed to get lithium and naphthalene to react. Lithium gives its valence electron to naphthalene which has higher electron affinity. In the resulting solution, lithium cations are paired with naphthalene anion radicals and they are coordinated by THF molecules (see Figure 2.3). [118–120]

The redox potentials of naphthalene and CNT are about 2.5 and 0.5 eV [5] respectively. When the prepared alkali solution is poured onto the CNTs, naphthalene anions give gradually their extra electrons to nanotubes (n-doping) and THF-dissolved lithium cations gather around negatively charged nanotubes. Consequently, the only role naphthalene has is to act as an electron transfer agent in this process, because neither lithium nor CNTs are soluble in THF. Now the nanotubes can be easily dissolved in polar organic solvents due to weakened tube-tube interactions. [122]

2.2.3 Alkali Solution for Doping

In addition to its separating ability, the alkali solution has been shown to modify the electronic structure of CNT. This has been proved by monitoring the optical properties of thin film CNT samples [4]. The same solution can be used to modulate the electrical conductivity of a bucky paper sample, too [5].

Alkali metal vapors are commonly used for n-type doping of CNT

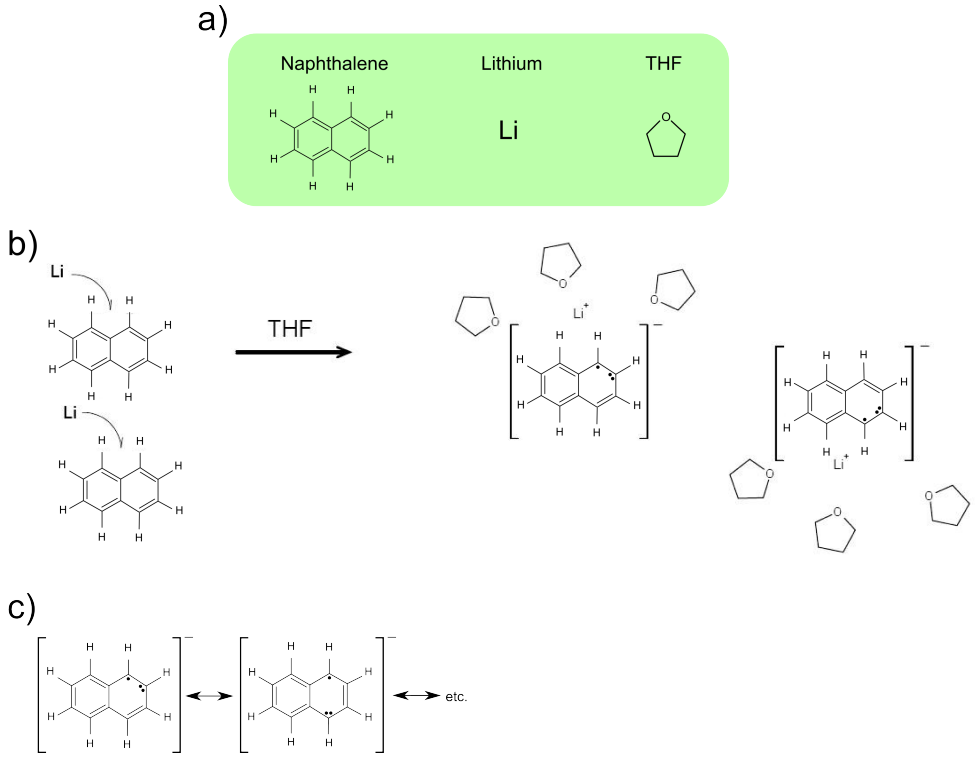

Figure 2.3: Electron transfer from lithium to naphthalene. a) Structural formulae of naphthalene, lithium and THF. b) Lithium gives easily its valence electron to naphthalene. Polar solvent THF stabilizes formed ionic pairs of naphthalene anion radicals and lithium cations. Naphthalene anion radical has many resonance structures and there is few of them drawn in c). Adapted from ref. [121].

FETs and the reversal from p- to n-type behavior has been confirmed by electronic transport measurements [1, 2]. This kind of direct electrical measurements have not been made earlier for individual CNTs exposed to liquid-phase alkali solution, which also is the main motivation for this thesis.

Chapter 3

Experimental Techniques

3.1 Essential Techniques Needed in CNT FET Fabrication

3.1.1 Electron Beam Litography

In this work, fine metallic patterns for the CNT FETs were made by commonly used electron beam (or e-beam) lithography method. Electrons have a wavelength so small that diffraction no longer defines the resolution of the pattern contrary to the case of light. Thus e-beam lithography provides a better resolution and accuracy than one of the most famous fabrication methods, optical lithography. [123]

In e-beam lithography the desired pattern is drawn by a beam of focused electrons which scans across a surface covered with a resist film sensitive to electrons. Exposed or non-exposed regions are selectively removed in the developing stage depending on the type of e-beam resist: Positive resists broke at exposed regions into fragments which can be easily dissolved in a developer solution. On the contrary, negative resists remain at exposed regions due to the radiation-induced polymer linking which creates a complex three-dimensional structure non-soluble in a developer. [123]

Created resist pattern can be used as a mask for patterned thin film growth, as shown in Figure 3.1.

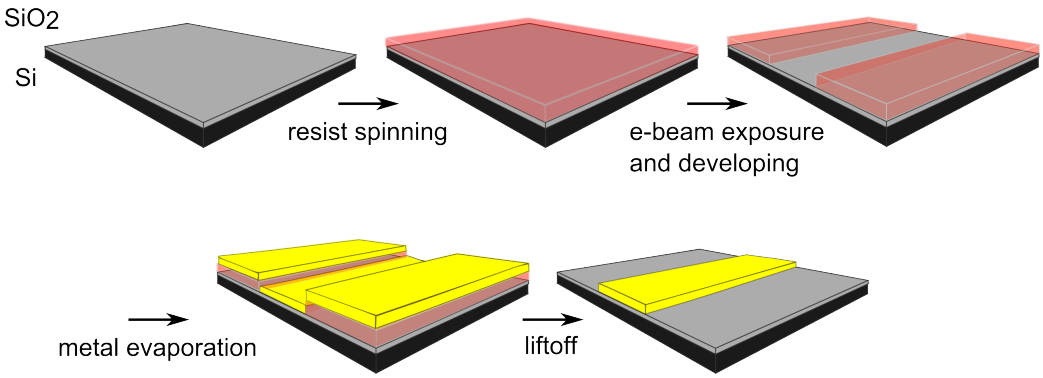

Figure 3.1: The stages of e-beam lithography. At first a thin resist layer is spun on a silicon chip. Then wanted pattern is written to the resist by e-beam writer and exposed (or non exposed) areas are rinsed off with developer. A thin metal film is evaporated on the chip and the regions on the remained resist layer are lifted off. The result is the wanted pattern of thin metal film on the chip.

3.1.2 Atomic Force Microscopy

Figure 3.2 shows a schematic representation of an atomic force microscope (AFM). Atomic force microscopy is one type of scanning probe microscopy method for measuring surface properties and/or profiles on a sub-nanometer scale. The attractive or repulsive forces between a sample and a sharp tip at the end of a cantilever cause the cantilever to bend. The bending is typically measured by using a laser beam reflected from the top of the cantilever into an array of photodiodes. Piezoelectric elements facilitating tiny and accurate movements enable the scanning of the selected area on the sample. The deflection of the cantilever during scanning is recorded producing a topographic image of the sample. [124]

AFM has a number of modes such as contact, non-contact, tapping, magnetic force, electrical force, and pulsed force modes. Tapping mode is the most widely used due to its gentleness and good resolution. In that mode, the cantilever oscillates in the vicinity of the sample near its resonance frequency so that the tip makes contact with the sample once during each cycle. Interacting forces between the tip and the surface decrease the amplitude of this oscillation. A feedback loop adjusts the height of the cantilever above the sample by maintaining the oscillation amplitude at a constant set-point value. The vibrating cantilever is scanned across the surface and the recorded feedback signal is used to identify the surface properties such as smoothness and topography. [124]

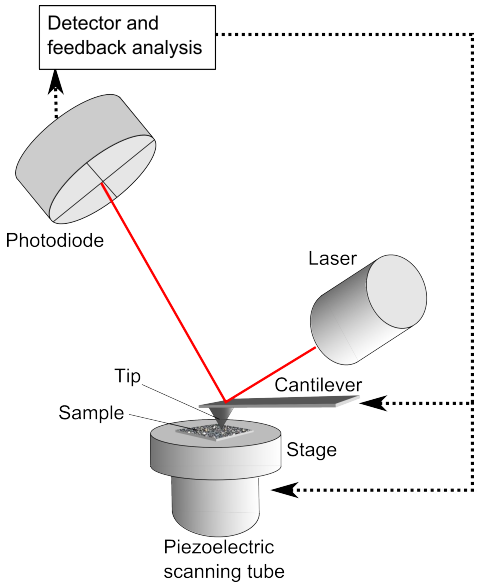

Figure 3.2: Schematic representation of an atomic force microscope (AFM). The forces between the sample and the tip cause the cantilever to bend. The bending is recorded with a laser reflected from the top of the cantilever into an array of photodiodes. The selected area is scanned through producing a topographic image of the sample.

3.2 CNT FET Fabrication

3.2.1 Substrate

The CNT FETs were fabricated on a smooth surface of a 500 µm thick highly p-doped single crystal silicon wafer. About 500 nm thick SiO_2 layer was made on both sides of it by low pressure CVD-method.

At first the wafer (a thin disk with a diameter about 15 cm) was cut into a few smaller pieces, cleaned in acetone, and then the oxidation process was done in a high temperature oven at 1100 °C under oxygen flow for 5 hours. After the oxidation the wafer was pre-cut into 6 mm $\times$ 6 mm detachable pieces (called chips). The pre-cutting was made with a silicon saw on the back side of the wafer and only halfway through its thickness. After the pre-cutting the wafer was cut into smaller pieces (called batches) containing 3 $\times$ 4 chips at most due to the limitations of the machines (e.g. the size of the sample stage inside the e-beam writer) used in the fabrication of CNT FETs. The silicon dust formed during cutting was cleaned off in hot acetone, after which the chips were rinsed

in isopropanol (IPA) and dried in a nitrogen flow.

3.2.2 Resists for e-beam patterning

The mask used in e-beam patterning was Commercial Microchem e-beam sensitive positive resist [125]. At first a batch of chips was pre-heated on a hot plate at 160 °C for five minutes to evaporate condensed water away from the surface. The first layer of 3 % polymethylmethacrylate (PMMA) dissolved in anisole was spin coated with a spinner (Bidtec SP100) at 3000 rpm. 2 % PMMA in anisole was then spun on top of that at 6000 rpm. The molecular weights of used resists were 495 000 and 950 000 creating about 100 nm and 60 nm layers on the substrate. After each spinning the batch of chips was baked on a hot plate at 160 °C for four minutes to evaporate solvent away and solidify the resist.

During the e-beam exposure an undercut was formed (see Figure 3.3), because the lower layer had smaller molecular weight and thus broke easier into smaller dissolving fragments. Such an undercut helps to prevent the resist sidewalls from being coated with thin metal film in the metallization step and makes the lift-off easier.

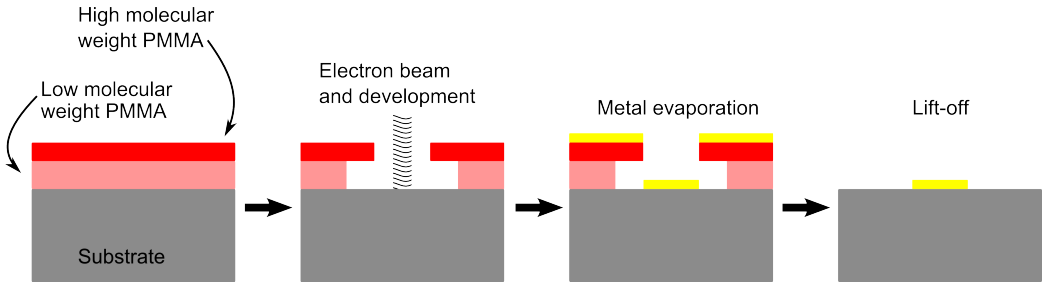

Figure 3.3: Dual layer resist leads to undercut formation which helps in the lift-off stage. The lower layer has smaller molecular weight and electron beam brokes it easier into smaller dissolving fragments than upper layer. In the developing step, the lower layer is dissolved faster than the upper one, which leads to undercut formation.

3.2.3 Pattern Exposure and Developing

Two different patterns were exposed on a chip. The first pattern was a base structure containing an AFM marker grid, larger markers for the alignment of the e-beam writer for the second pattern exposure, 28 bonding pads,

and electrodes from the bonding pads to the marker grid (see Figure 3.4). The base structures were prepared on the batches of chips (one base structure per one chip). Then a chip was broken off from a batch and the nanotubes were deposited on that chip. The nanotubes were located with an AFM and after that the electrodes from the nanotubes to the outer electrodes were drawn in the second exposure.

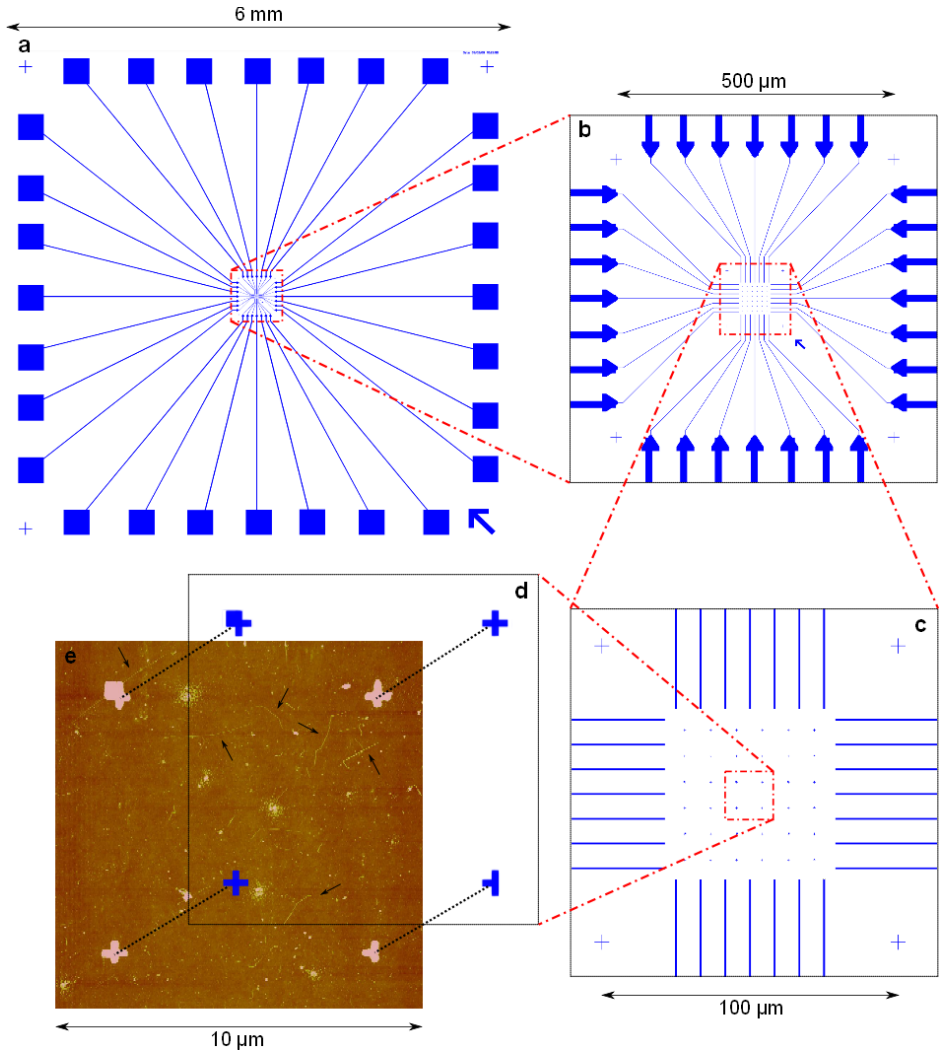

Figure 3.4: The base structure. (a) The whole structure (6 × 6 mm), bonding pads on the edges and outer alignment marks (crosses) on the corners. (b) Enlarged image of the base structure with inner electrodes and middle alignment marks. (c) A 6 × 6 alignment mark matrix for AFM imaging in the middle of the base structure. (d) A set of alignment marks. (e) AFM image from the same area. Deposited nanotubes are marked with arrows.

The base structure and the overlay pattern were designed with Elphy Quantum 4.0 lithography software. The same software was also used to manage exposure parameters and pattern overlay alignment. The designed patterns were exposed with Raith e-LiNe scanning electron microscope (SEM) which can be used as ultra-high resolution electron beam writer. This SEM has a thermally assisted field emission gun and a 45 mm laser interferometer stage. Its imaging resolution is below 10 nm and minimum lithography feature size below 20 nm. A stitching accuracy and an overlay accuracy are below 40 nm. [126]

The resists of the exposed areas were removed by immersing the chip in developer 1 (1:3 methylisobutylketone/isopropanol) for 60 seconds and after that in developer 2 (1:2 methyl glycol/methanol) for 5 seconds. Developer 2 is more aggressive and it is used for removing residuals from the surface of the developed areas. At last the chip was rinsed in IPA and dried in a nitrogen flow.

3.2.4 Metallization and Lift-Off

A thin metal layer was deposited on the chip under high vacuum by Balzers BAE 250T HV electron beam evaporator. Electron beam evaporation is one type of physical vapor deposition method and a typical setup is shown in Figure 3.5. A high current passes through a wire filament and heats it up to a high temperature. At this high temperature electrons are emitted from the surface of the filament and accelerated, directed, and focused to hit the source material that heats up and evaporates. Evaporated material flows to the target as line-of-sight principle and the thickness of the thin film is controlled by the shutter.

Two different metals, titanium (5 nm) and palladium (15 nm), were used for the base structure. Titanium was used below palladium to improve the adhesion of the latter. The evaporation rate was about 0.1 nm/s for both metals.

Non-exposed areas with resists and the evaporated metal on top of it were removed in lift-off. The chip was put in hot acetone for about 10 min to dissolve the resists and extra metal was then easily removed by injecting hot acetone with high pressure on the chip. The chip was then rinsed in IPA and dried in a nitrogen flow.

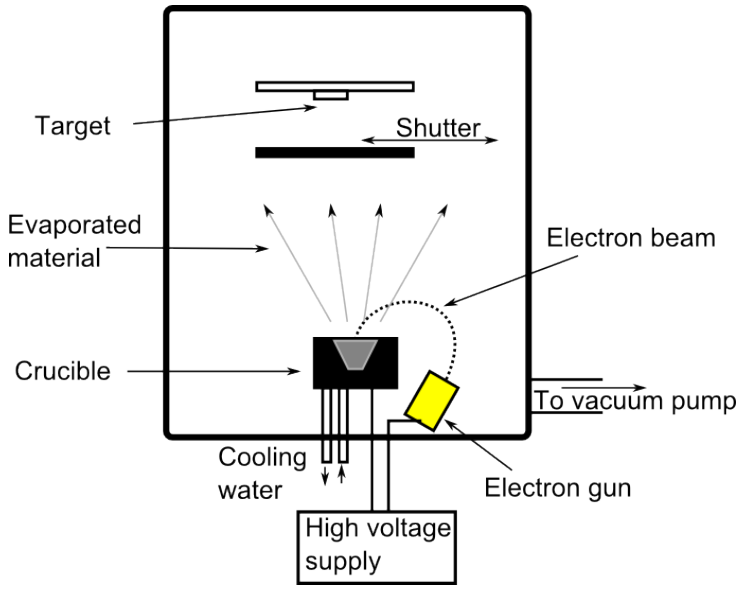

Figure 3.5: Electron beam evaporation setup.

3.2.5 Deposition of Nanotubes

One chip was broken off from the batch of chips with the base structures, cleaned in hot acetone, rinsed in IPA, and dried in a nitrogen flow. Commercial Nanocyl 1100-series single-wall carbon nanotubes [127] (average diameter of 2 nm) made by catalytic chemical vapor deposition (CCVD) were dissolved in 1,2-dichloroethane and sonicated for 20 minutes (Finnsonic m03 20) to separate bundled nanotubes. Sonication is quite a harsh separating method and it can induce defects and shorten the tubes [128]. Alkali solution can be used to separate the tubes gently and efficiently [117], but the tubes were not intentionally brought in contact with that solution before measurements. After separation the nanotubes were deposited on the chip by spinning 5-10 droplets of the nanotube solution at 1500 rpm for 60 seconds. The droplets were added on the chip with a pasteur pipette when the spinner was on, so the tubes will not have too much time to attach on the surface and the density of the tubes is not too dense.

3.2.6 AFM-Mapping and Second Exposure

The imaging system was Digital Instruments (Veeco Metrology Group) Nanoscope Dimension 3100 AFM and the used imaging mode was the

tapping mode. The marker crosses in the marker grid are 7 µm apart from each other, so when taking 10 µm by 10 µm AFM images, one can locate the deposited nanotubes relative to the crosses (see Figure 3.4). When good tubes were found, closer images of them were taken to estimate the cleanliness and dimensions of the nanotubes. The profile of the cantilever tip is round, so the width of the nanotube is much larger in the image compared to the real value. This is why the diameter of the nanotube was determined from the height profile of the nanotube by measuring the height at a few different points and then calculating the mean value of the measured values (see Figure 3.6).

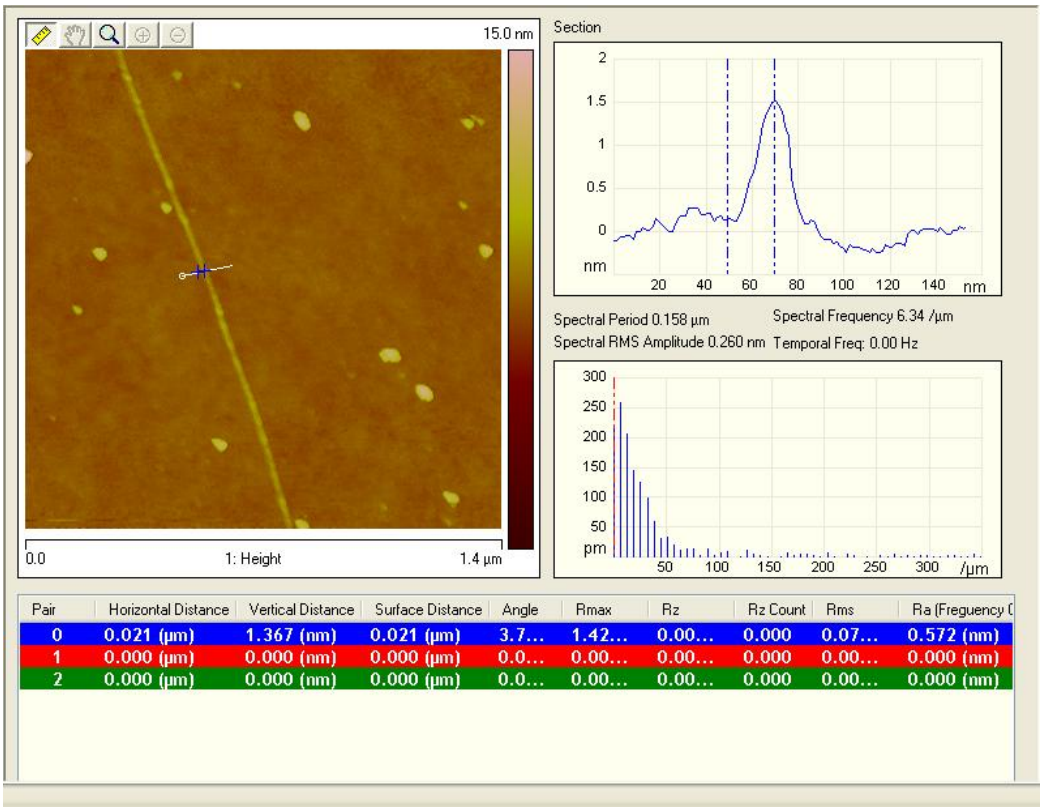

Figure 3.6: Screenshot of the program that was used to determine the height of the nanotube from AFM images. The height profile of the drawn line is shown in the upper right corner.

The saved AFM images were opened with Raith Elphy Quantum pattern designer and the electrodes (in other words, metallic contacts to the ends of the nanotube) were designed for the selected nanotubes. Two wires were needed for the back gate per chip (explained later in section

3.2.7) and when using two electrodes for each CNT FET, up to 13 FETs can be designed per chip.

The second exposure was done in a similar way as for the base structure. The alignment markers of the base structure were used in the e-beam exposure step to get the overlay pattern on the right place. The drawn features were smaller in the second exposure, so the aperture size was only 30 µm. In the metallization step titanium was left out from the receipe and only a 25 nm thick palladium layer was evaporated on the chip. This change was done because palladium makes a better contact with a nanotube than titanium.

After the lift-off, an optical microscope was used to check the success of the lift-off stage and alignment. The width of the electrodes can vary a lot depending on the many parameters (resist thickness and quality, exposure power and time, development time, etc.), thus the channel lengths (see Figure 3.7) of the CNT FETs had to be determined by AFM. Sometimes the alignment did not succeed properly and the whole overlay pattern shifted to some direction. If the shift is significant, some of the devices may not work, because the electrodes are not on the nanotubes.

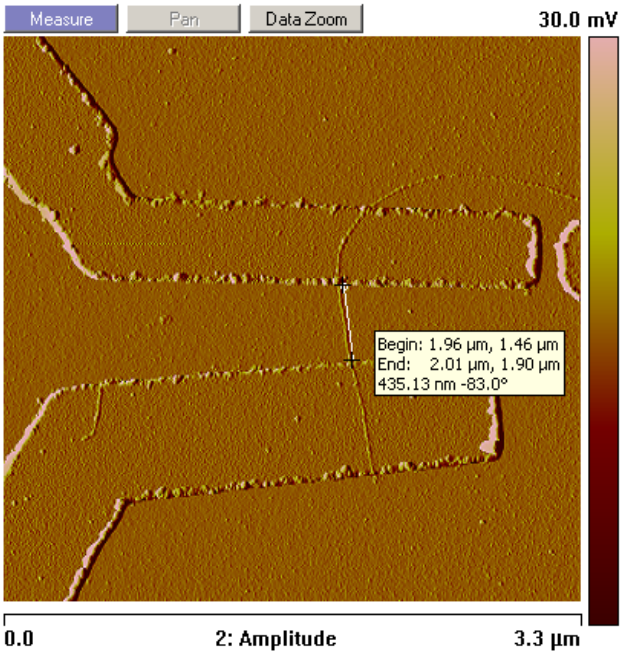

Figure 3.7: The channel length of the CNT FET is the length of the nanotube between the electrodes, which is easy to determine with AFM.

3.2.7 Bonding

To ease the handling and measurement of the prepared devices on the chip, it was glued on a chip carrier with varnish (see Figure 3.8). A plain chip goes too deep into the carrier so that imaging of the devices with AFM is impossible afterwards, so two small washers were glued under the chip to raise it a little. A Kulicke & Soffa 4523A thin wire bonder was used to connect the electrodes of the devices to the chip carrier with thin aluminum wires. The silicon base of the chip can be used as a back gate, so two electrodes of the carrier were bonded to the edge of the chip and connected to the silicon substrate with silver paint. The functionality of the back gate is now easy to test by putting a voltage between these two electrodes and monitoring the current going through the chip. If there is a very small current or no current at all, at least one of the back gate connections is bad.

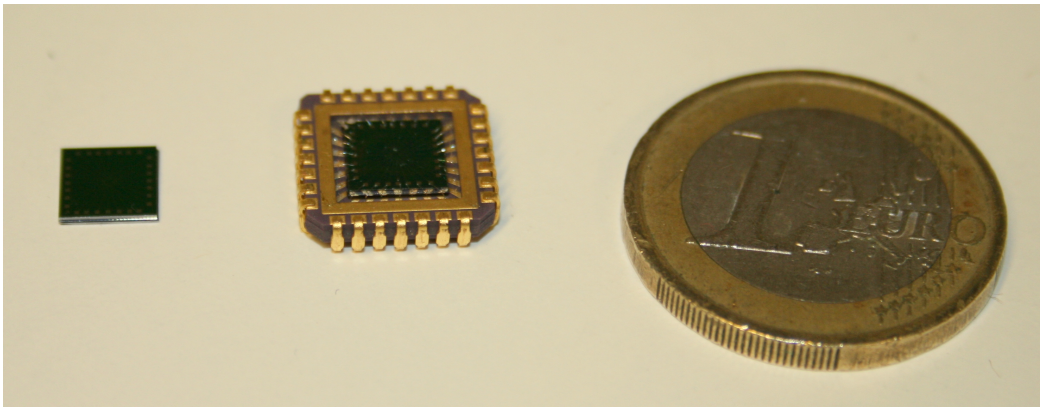

Figure 3.8: A chip with a base structure on the left. The biggest structures, bonding pads, can be seen on the edges of the chip. In the bonding stage, the chip is connected to the chip carrier by thin metal wires (in the middle). The coin on the right acts as a scale bar for the previous.

After bonding the chip carrier was placed in a socket mounted on the metallic measurement box. The connections between this box and other measurement equipments were made with BNC cables.

3.3 Alkali Solution

Because lithium reacts easily with oxygen and humidity, an alkali solution had to be prepared and handled under inert atmosphere either in nitrogen

or in argon. Used reagents and glassware were dried to minimize the amount of oxygen and water in them.

At first 400 mg of solid naphthalene was weighed out into a three-neck flask. Then the flask was connected to a vacuum pump (line) which removed air and humidity from naphthalene.

Tetrahydrofuran (THF) was dried by refluxing it under nitrogen gas atmosphere with sodium for more than one hour. Then benzophenone was added and the solution was refluxed until the color of it was deep blue (see Figure 3.9). Sodium reacts easily with water and comprises sodium hydroxide (NaOH). Benzophenone and sodium form a colored complex which is blue if the solution does not contain water, and brown if there is water.

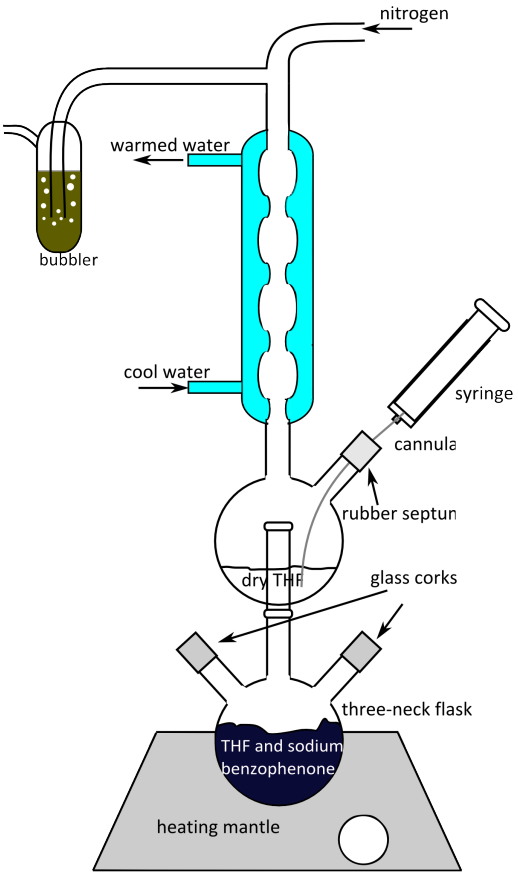

Figure 3.9: Sodium benzophenone and THF were refluxed under nitrogen atmosphere. Clean THF was vaporized and this vapor was condensed in a condenser and trickled in the upper flask, where it can be suctioned by a syringe.

30 ml of dry THF was measured into a glass syringe and inserted into the flask containing dried naphthalene. A lithium wire (diameter ca. 5 mm) was taken out of mineral oil and cutted into small pieces and weighed out 35 mg. Then lithium was rinsed in petroleum ether (evaporates off fastly, bp. 40-60 °C) to remove mineral oil, and put into the THF and naphthalene solution. There was no reaction between naphthalene and lithium yet, because more energy (heating) is needed to get over the threshold of the reaction. The mixture was refluxed at ca. 60-70 °C with a magnetic mixer for about half an hour. In this stage, lithium donates its valence electron at least partially to naphthalene and dissolves in the solution and the colour of the solution turns black green as shown in Figure 3.10 (discussed more precisely in section 2.2.2). If there was any air or water in the flask, the colour of the solution turned brown.

Figure 3.10: Fresh, dark green alkali solution in a Rotaflo flask.

Doping of CNT FETs was done in a glove box and the solution had to be brought into the glove box through a vacuum chamber, thus the solution was transferred into a two-neck Rotaflo flask which can survive in vacuum. The Rotaflo flask was filled with argon and a rubber septum was put to its side neck with parafin tape. There was a rubber septum in the three-mouthes flask containing the alkali solution, too. The solution was transferred into the Rotaflo flask by creating a pressure difference between the flasks and connecting them with a thin metallic cannula (see Figure 3.11).

When interpreting the results of this work, one has to take into account that the quality of the alkali solution depends highly on the preparation, treatment, and storage conditions (the purity of the reagents and the glassware, the relative humidity, light exposure, etc.). Thus the mentioned

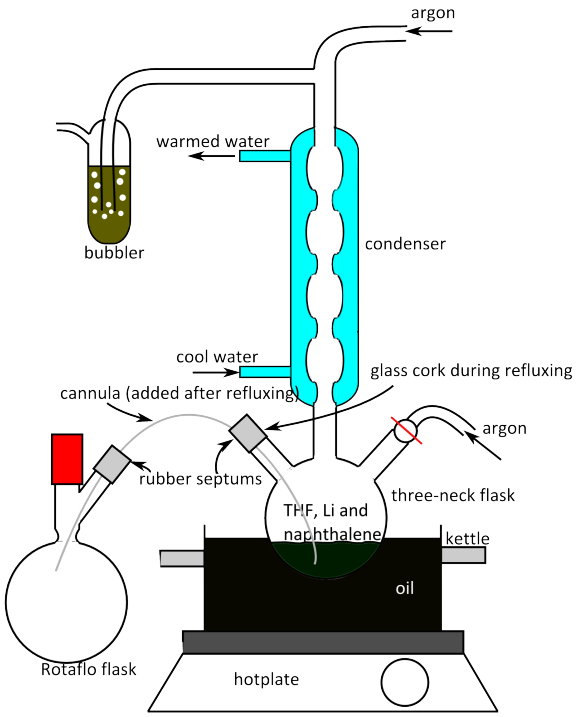

Figure 3.11: Refluxing setup. The reaction between lithium and naphthalene can occur when the solution is heated. The condenser prevents the loss of THF. Prepared green alkali solution is cannulated from the three-mouth flask into the Rotaflo flask by the aid of pressure difference between the flasks. The pressure difference is created by closing the route to the bubbler and opening the lower argon line.

concentrations of alkali solutions are only estimates. Fresh alkali solution is initially dark green, but it was noticed to change color to light brown in a few weeks. Both THF and polyaromatic radicals (such as naphthalide anion) are known to be light sensitive, which is probably the reason for the change of color. Metallic lithium reacts also easily with oxygen and water forming lithium oxide (Li_2O) or lithium hydroxide (LiOH). Small amounts of oxygen and water in the glove box can also cause this color change of alkali solution in a long term.

Chapter 4

Measurements and Results

The electronic transport properties of CNT FETs depend highly on the ambient environment of the device, so ambient gas and all components of the doping solution have their own effect on the properties of CNT FETs. A multistep measurement series was carried out, where the effects of ambient gases and each component of the alkali solution on the electronic transport properties of CNT FETs could be carefully determined. In addition, the sensor-like behavior of CNT FET was tested by measuring the gate response during the doping process in real time. All measurements were done at room temperature.

The real time measurements were performed for a CNT FET when it was in alkali solution. Since concentrated alkali solution is a conducting polyelectrolyte, the transport characteristics of the CNT FET can be measured during the doping process only if alkali solution is diluted enough to reduce its conductivity below the conductivity of the CNT FET. Thus resistances of different dilutions in different setups were measured to find out a suitable concentration for the real time measurements.

The first section of this chapter presents the measurement setup. After that the resistance measurement of the alkali solution is described. Finally, the measurements done with CNT FETs are discussed. The main results are presented and analysed along with the description of the measurements.

4.1 Measurement Setup

The measurement setup (see Figure 4.1) was the same in all CNT FET measurements. National Instruments BNC-2090 data acquisition board (DAQ) has two output and 16 input channels. The outputs produce

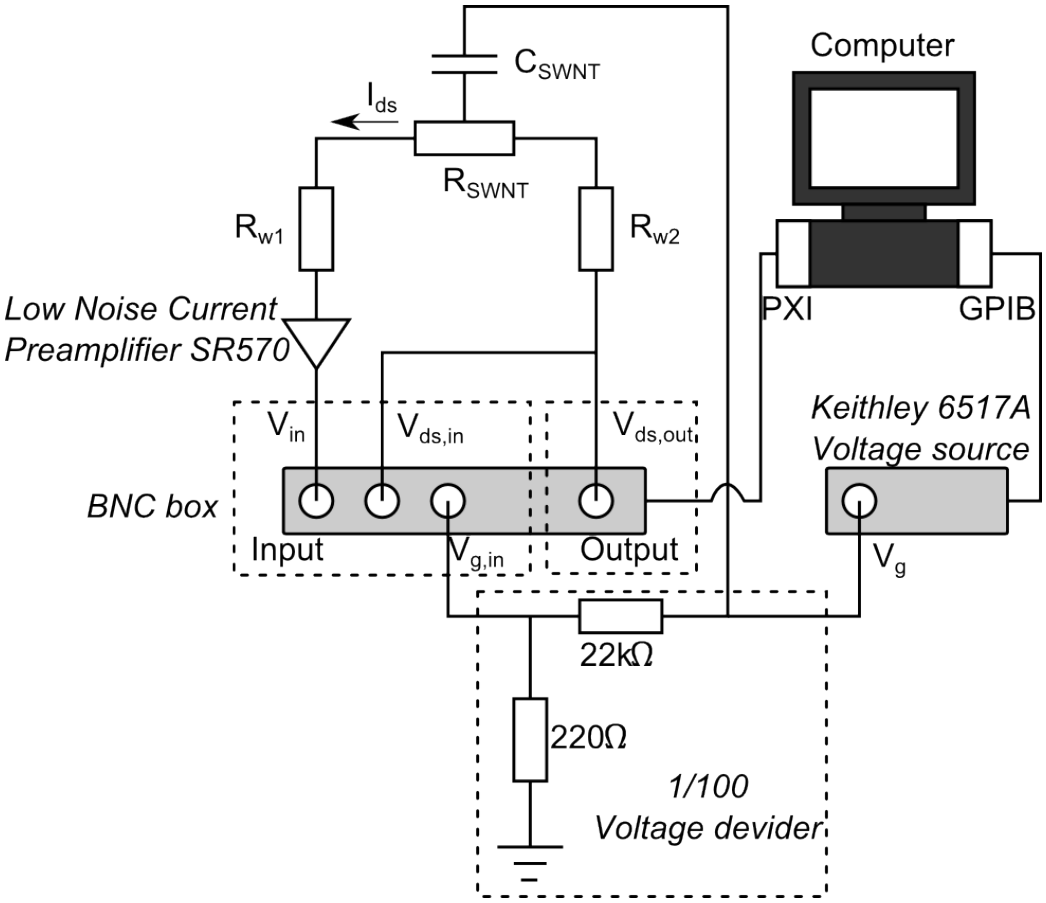

Figure 4.1: The measurement setup.

voltages up to ± 10 V with a 5 mV step size. One of the output channels was used for the drain-source voltage (V_{ds}). Keithley 6517 Electrometer supplied a voltage for the back gate (V_g), because the BNC board cannot provide high enough voltages for that purpose. Keithley 6517 can apply voltages up to 1000 V (the highest needed was only 25 V) and its step size is also 5 mV.

The inputs of the BNC board collected the data in volts and sent it to the computer which multiplied the values by the preset gains and saved the data. The drain-source current (I_{ds}) was converted into voltage (V_{in}) and amplified by Stanford Research Systems SR570 Low Noise Current Preamplifier. The BNC board can read only voltages smaller than ± 10 V, so the gate voltage had to be reduced by 1/100 voltage divider.

The BNC board was controlled via PXI and Keithley 6517 via General Purpose Interface Bus (GPIB) from the computer. All measurements were

done in Labview environment and data analysis was performed with a data analysis and graphing software OriginPro 7.5.

The resistances of wires (R_{w1} and R_{w2}) can be ignored, because they are usually a few tens of ohms, whereas the resistance of the nanotube is in order of kilo-ohms.

4.2 Resistance of Alkali Solution

The measurement setup used in the resistance measurements of the alkali solution was the same as in CNT FET measurements (see Figure 4.1), but nanotube was replaced with alkali solution and the voltage source Keithley 6517 Electrometer was disconnected (otherwise used for CNT FET back gate).

At first a dilution series with a dilution factor 10 was prepared from the original alkali solution ($c \approx 170$ mM) into 2 ml vials with micropipettes. THF was used as a diluting agent. Lithium concentrations in the prepared dilutions were 170 mM, 17 mM, 1,7 mM, 170 µM, 17 µM and plain THF.

The resistance of the alkali solution was measured for four different setups: between two metallic wires, opposite electrodes of the base structure, adjacent electrodes of the base structure, and electrodes of a broken device (see Figure 4.2).

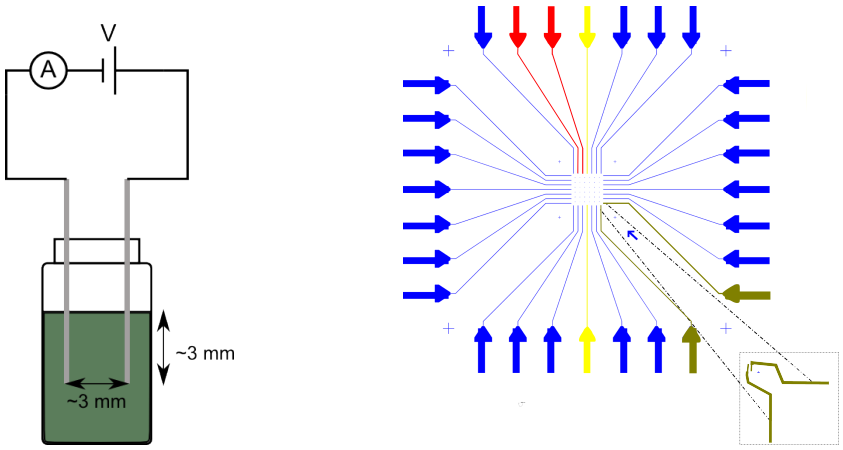

Figure 4.2: The resistance of alkali solution was determined for four different setups. The wire setup on the left. The enlarged image of the base structure on the right, where opposite electrodes are yellow (with shortest distance about 45 µm), adjacent electrodes are red (with shortest distance about 7 µm) and electrodes of a broken device are green (on a different chip, shortest distance about 400 nm).

The first measurements were done with a wire setup which had two metallic wires put into the vial containing diluted alkali solution, and the current through the solution was measured as a function of applied voltage (V=+1...-1). The resistance of that dilution was then determined from the slope of the formed linear graph. This was repeated for each dilution and the wires were washed in THF between each measurement.

One could expect that the resistance would decrease when increasing the concentration of the electrolyte. In these measurements resistance increased unexpectedly about one order of magnitude, when concentration was increased from 170 µM to 1,7 mM (see Figure 4.3). Because of this, more dilutions were prepared between 170 µM and the original concentration, 170 mM, to get a better image of that phenomenon. To be sure that there was no error in the preparation of the dilutions, the same behavior was confirmed also with a new dilution series, too. The explanation for the observed resistance maximum could be a phenomenon called ion pairing. Free ions can form neutral ion pairs or clusters in certain concentrations in low-permittivity solvents, such as THF ($\epsilon_r = 7,58$), causing a conductance minimum (resistance maximum) in the conductometric curves. [129,130]

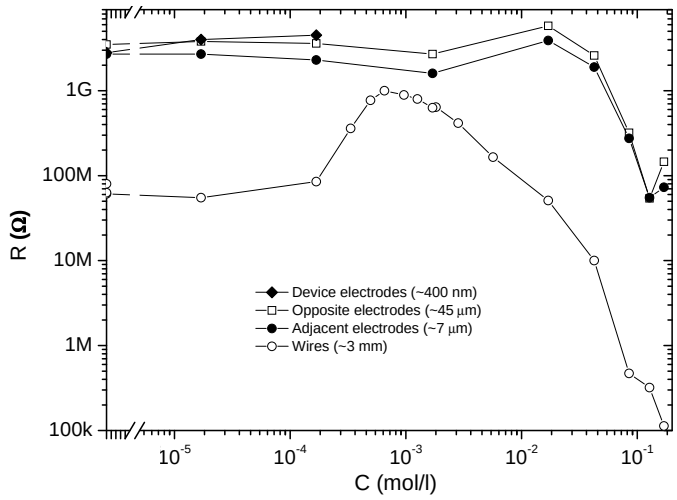

Figure 4.3: Resistance of active solution in different setups. Note that the scales are logarithmics.

After the wire test the resistances of different dilutions were measured between opposite electrodes of the base structure and between adjacent

electrodes of the base structure. A clean chip with the base structure was bonded to a chip carrier and a home-made flow chamber was mounted on that chip to make the exposure of the center area to a liquid possible, while the bonding pads and edges of the chip stay dry (see Figure 4.4). At first PMMA was used as a sealing between the chip and the chamber, but it was noticed to dissolve in THF, so it was changed to a plastic wrap.

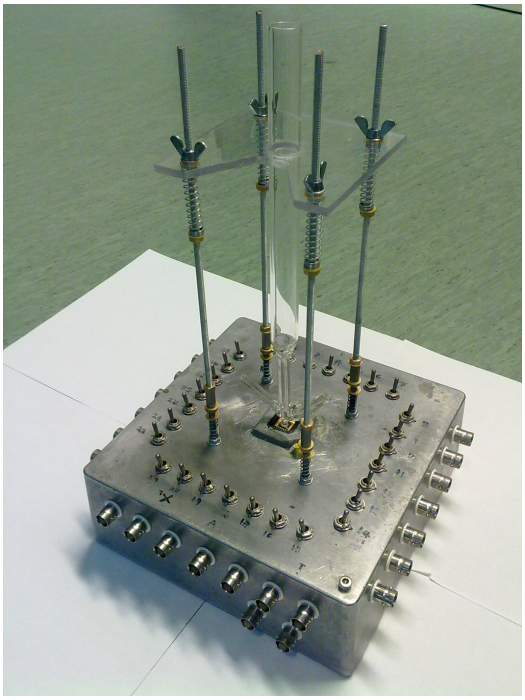

Figure 4.4: A home-made flow chamber mounted on the chip for liquid phase measurements.

The trend of the resistance in these setups was quite the same as with the wires, but the resistance was about one order of magnitude bigger (gigaohms) and the resistance maximum was smaller and shifted somewhat to higher concentrations, see Figure 4.3. The resistance measurements of the base structures were done with the same dilution series about half a month later than the measurements with the wire setup, so the quality of the alkali solution could change a little (e.g. reactions between the alkali solution and air/humidity) causing the shift of the maximum. The resistance between the wires was smaller compared to the base structure probably due to the different geometries of the setups (areas, distances, etc.) or the quality of the alkali solution.

Finally, the resistances of three most diluted solutions (170 µM, 17

μM and 0 M) were measured for the device which was confirmed to not conduct anymore (the nanotubes of CNT FETs can easily broke by careless handling, such as poor grounding, electrostatic discharges, etc.). The setup was the same as in the previous measurement, but the chip was replaced with another chip having this broken device. This measurement gave the most realistic values for the resistance of the alkali solution and how it will affect the real time measurements done with working devices. Based on the results of these resistance measurements (see Figure 4.3), 1/1000 dilution (170 μM) was chosen for the real time measurements due to its high enough resistance (above 10 GΩ).

4.3 CNT FET Measurements

This section presents the preliminary measurements, how to measure typical transport properties of a CNT FET, what kind of flow of the measurement series was planned to study the doping process, and finally what results were found.

Tables A.1 and A.2 in Appendix A represent the essential information of the prepared devices, such as the diameters and the types of the nanotubes. The full names of the devices are quite long, so the devices occuring in the text (devices S1, S2 and S3) are named with a short abbreviation shown in the tables.

4.3.1 Preliminary Measurements

At the beginning of the measurements the setup and the devices had to be tested. At first, a measurement program was designed with Labview and the I–V curves of a few normal resistors with known values were measured and their resistances were calculated from the formed linear graphs. This helped to check the measurement system in case of rough errors in e.g. applied voltages which could destroy the delicate CNT FETs. Usually the test measurements contained a back gate test, a leakage test, and a rough working test of devices.

In the back gate test the current through the back gate was measured as a function of applied voltage. If the calculated resistance was low enough, both back gate contacts were good. Even a resistance of one mega-ohm can be low enough, because there is no current flowing through the back gate during the measurements, but the back gate is only charged slowly.

In the leakage test the resistances between the back gate and the electrodes were measured. A device with a leaking electrode is practically useless, because the currents between the leaking electrode and back gate interrupt the measurement of I_{ds}.

The rough working test was either a plain resistance test between the electrodes of the device (V_{ds} was scanned from -50 mV to +50 mV) or it might also involve a fast test with the back gate, where the back gate voltage was scanned quite fast e.g. between +10 V and -10 V with a constant V_{ds}. If the device worked, its resistance was measured from tens of kilo-ohms to tens of mega-ohms at $V_g = 0$ V. The resistance test is faster, but if the device is in its OFF-state during the test measurement, one can classify working devices into non-working devices. That is the main reason why the test with back gate was usually used.

4.3.2 Measurement of Typical Characteristics

The main characteristics of CNT FETs can be read from the I_{ds}–V_g graphs as discussed in Section 1.3.3. The drain-source voltage V_{ds} was set to constant and then the gate voltage V_g was swept back and forth between +25 V and -25 V. The step size of V_g was 20 mV and point rate 65 Hz. Typical I_{ds}–V_g curves are shown in Figure 4.5. Due to chirality, a fraction (1/3) of nonspecifically prepared carbon nanotubes are metallic [22], so about the same fraction of the prepared CNT FETs had metallic behavior and were useless in these measurements. The current through metallic CNT FETs has no dependence on the back gate voltage, so they work only as a resistive wire (see Figure 4.5).

The resistances in ON and OFF states were determined by setting V_g to the constant value where the device was in ON (or OFF) state. Then V_{ds} was swept from +50 mV to -50 mV and the resistance of the device was determined from the formed linear I_{ds}–V_{ds} graph. Currents were usually in the order of nanoamperes or smaller in OFF states of CNT FETs, so they were very sensitive to errors caused by e.g. imperfect zeroing of the current preamplifier. The corrected OFF state current is $I_{ds,corr} = V_{ds}/R_{OFF}$, where R_{OFF} is the resistance of the channel in the OFF state and V_{ds} is the drain-source voltage during the gate sweep.

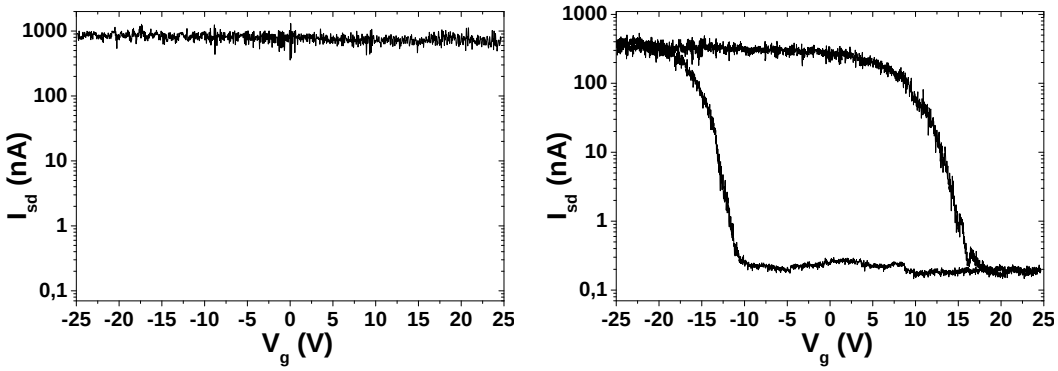

Figure 4.5: Typical I_{ds}–V_g characteristics of metallic (on the left) and semiconducting (on the right) CNT FETs.

4.3.3 Flow of the Measurement Series

The effects of ambient gas (air and argon) and the different parts of the alkali solution (THF, naphthalene and lithium) on the behavior of the CNT FET were determined by the measurement series shown in Figure 4.6.

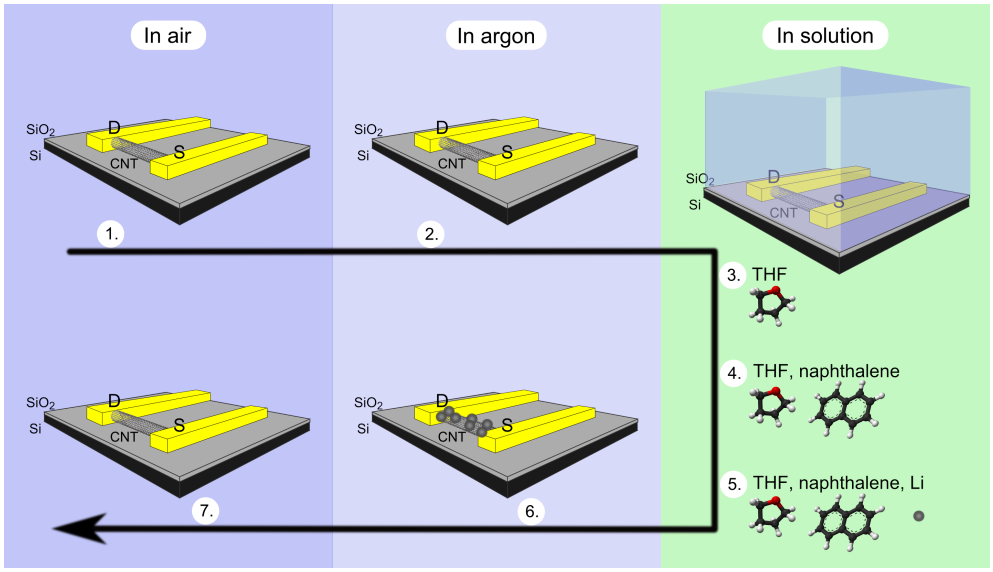

Figure 4.6: The outline of the measurement series. The transport characteristics of CNT FET were first measured in air (1) and in argon (2). Then the flow chamber was mounted on the chip and the behavior of the CNT FET was measured in different solutions in a row: in plain THF (3), in THF and naphthalene (4), and finally in THF, naphthalene, and lithium (5). After that the transport characteristics were measured again in argon (6) and also in air (7).

The drain-source voltage V_{ds} was kept at constant value +34 mV during the whole measurement. At first the gate response was measured in air. After that the flow chamber was mounted on the chip and the whole setup was brought inside the glovebox and it was kept there overnight before measuring the gate response again. Oxygen and humidity levels inside the glovebox were below 150 ppm during the measurements.

The transport characteristics of device S1 were measured in four different solutions in a row: in plain THF, in THF and naphthalene (two different concentrations: 10 mM and 100 mM), and finally in diluted alkali solution (170 µM with respect to lithium). Every stage lasted until the curves became stable (at least 30 min) and the gate voltage was sweeped (0 V$\rightarrow$ +25 V $\rightarrow$ -25 V $\rightarrow$ 0 V) at least four times per each solution. Solutions were changed at $V_g = 0$ V, when the gate sweeping was at a pause. The measurement data was used to interpret the effects of different solutions, but the data got from the exposure to the alkali solution gave information about the time-dependence of the doping process (discussed later).

After the liquid-phase measurements, the device was rinsed thorougly with THF and dried in an argon flow and then the gate response was measured again in argon. Then the device was brought out of the glove box and cleaned with distilled water, dilute HCl, and IPA to remove lithium oxide (Li_2O) and lithium hydroxide (LiOH) that might have formed on the nanotube, dried in a nitrogen flow, and measured in air. This stage was so critical that devices often stopped working. This phenomenon resulted possibly from the intense reactions happening on the nanotubes covered with lithium.

Motion of lithium ions through the side-wall of the nanotube is energetically unfavorable [131], but they can easily diffuse to the interior through the defects or the open ends of the nanotube [132, 133]. The CNT material for the devices used in this study was sonicated in dichloroethane to separate the bundled CNTs. Sonication is known to introduce defects to the side-walls of the nanotubes [128], so it is justified to assume that some lithium ions diffuse to the interior of the nanotubes during the doping process. When a doped device is taken out from the glovebox and comes into contact with oxygen or water, strong exothermic reactions between lithium and oxygen or water can result in the unwrapping of the nanotubes [134] and thus damage the devices.

The measurement methods improved during this study, which is usual in experimental research. The measurement series described above was fully performed only on device S1. Device S2 was measured similarly as

S1, but the concentration of lithium was about four times bigger. Device S3 was not measured in solutions, but just before and after exposure to 170 µM alkali solution in argon.

4.3.4 Changing the Ambient Atmosphere

The measurements shows that the change of the ambient atmospere around the nanotube doesn't substantially affect the transfer characteristics of CNT FET (see Figure 4.7).

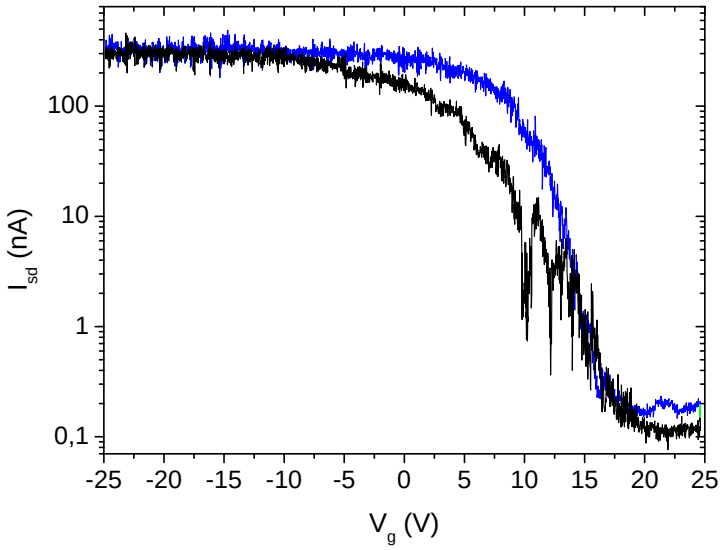

Figure 4.7: The transfer characteristics of device S2 in air (black) and in argon (blue) before doping shows that the change of the ambient atmosphere has no noticeable effect on CNT FETs.

All measured semiconducting CNT FETs remained p-type, while threshold voltages and OFF-state currents varied a little. A possible reason for the slight variation of the threshold voltages is a number of water molecules which are located on the surface of the nanotube and proposed to affect the gate response of carbon nanotubes by charging and locally screening the electric field [73,75]. Thus water desorption from the surface due to the low humidity level inside the glovebox is supposed to cause the small shift in threshold voltage. Respectively, errors of OFF-state currents can originate e.g. from the variations in the calibration of the measurement

setup between different measurements. Relative errors of very small OFF-state currents are so big that errors cannot be perfectly corrected by error calculations (shown in section 4.3.2).

Although the devices were brought inside the glove box through a vacuum chamber, there was still a small amount of oxygen and water on the nanotube, because a complete removal of oxygen needs heating combined with high vacuum [135]. This means that the immediate environment of the nanotube stays the same. Argon has been shown to have no noticeable doping effect on CNTs [135], which is also supported by the observed unchanged behavior of CNT FET during the change of the ambient atmosphere.

4.3.5 Effect of THF and Naphthalene

The gate response of CNT FETs changed a little when THF was added on the FETs (Figure 4.8). The change is similar to what has been observed in reference [136]. The gate response of CNT FET in acetone shows pronounced ambipolar behavior which may arise from the strong dipole moment of both THF and acetone. The addition of naphthalene had not any significant effect on the transport properties compared to the measurements done in THF.

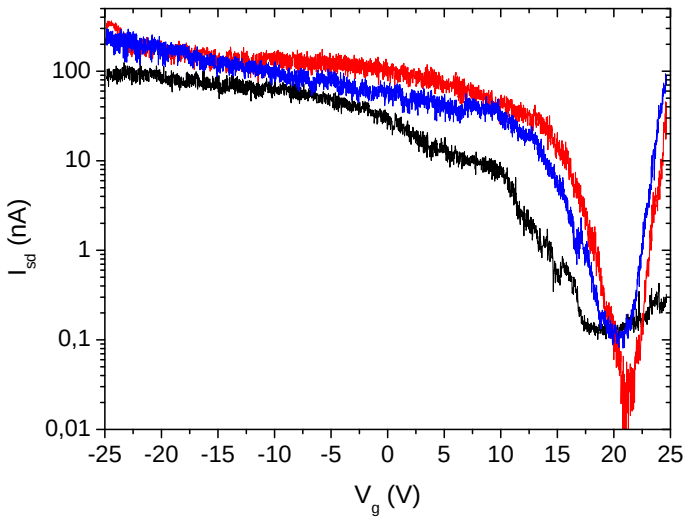

Figure 4.8: The transfer characteristics of device S1 in argon (black), in THF (blue), and in THF and naphthalene (red).

4.3.6 Doping by Alkali Solution

The addition of alkali solution changed dramatically the transport characteristics of CNT FETs, as can be seen in Figure 4.9. Before exposure device S1 exhibited p-type behavior with an ON/OFF ratio of 6 $\times$ 10^2 and after the exposure the type was changed to n-type with an ON/OFF ratio of 2 $\times$ 10^2. The subthreshold slope was qualitatively the same in both cases (about 5000 mV/dec).

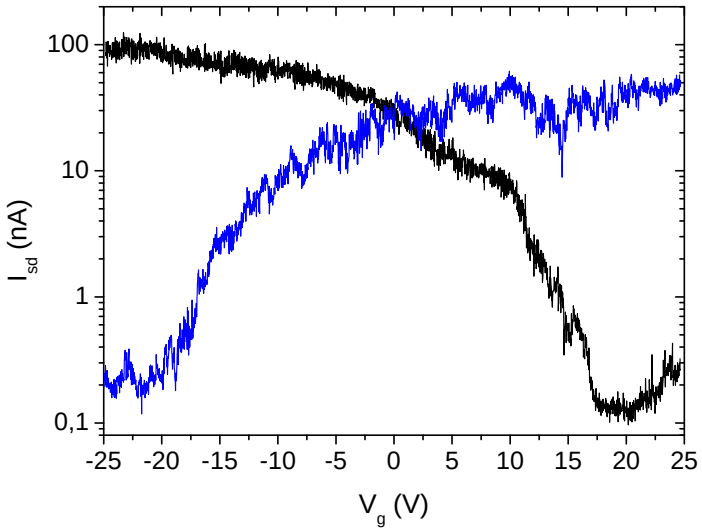

Figure 4.9: Device S1 in argon before (black) and after (blue) exposure to alkali solution. A clear change from p- to n-type can be seen.

This clear change from p- to n-type was observed in total with three devices. The ON/OFF ratio of device S2 was about 10^3 in argon before exposure and it was the same in the alkali solution during exposure, but when measuring it in argon after doping, the ratio was decreased to 10^2. Device S3 kept its ON/OFF ratio and subthreshold slope in the same orders of magnitudes.

These observations prove that neutral naphthalene dissolved in THF has no influence on the carbon nanotube. Thus the reduction of the carbon nanotube from p-type to n-type require lithium to reduce naphthalene and form naphthalide (negatively charged naphthalene) which in turn reduces the carbon nanotube. The role of naphthalene is only to transfer electrons from lithium atoms to the carbon nanotube, as a previous study

suggests [122].

4.3.7 Time-Dependence of Doping

The time-dependence of the doping was monitored for device S1 during the exposure to 170 µM alkali solution. The whole process lasted about 160 min and Figure 4.10 shows clearly, how the behavior changed gradually from clear p-type through ambipolar interphase to clear n-type.

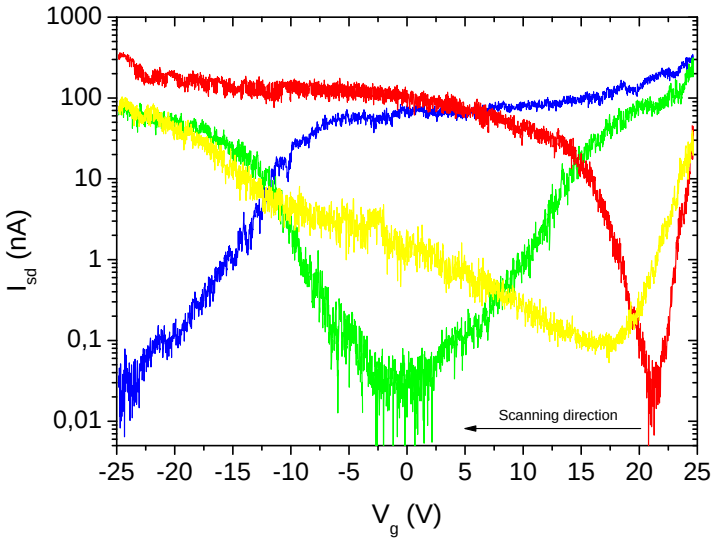

Figure 4.10: Time-dependence of doping in rainbow colors. Device S1 in THF and naphthalene (red), in alkali solution 5–11 min (yellow), 104–110 min (green), and 159–165 min (blue).

The real-time response of the CNT FET during exposure to active solution was measured (see Figure 4.11) [59]. A device was first confirmed to be a typical p-type CNT FET in argon and then the transfer characteristics were measured in 100 mM naphthalene in THF. The type was noticed to change to ambipolar with the p-type side dominating (see inset in Figure 4.11). Then the gate voltage was positioned at -5 V, where the CNT FET was in its ON-state on the p-type side and the current response during the addition of 170 µM alkali solution was measured as a function of time. When adding the solution on the device, the current gradually decreased and leveled out in the OFF state of the n-doped CNT FET within 20 min.

The change in current was over three orders of magnitude in both real time measurements proving clear response to the change of the conditions, which is one of the most important properties of a sensor.

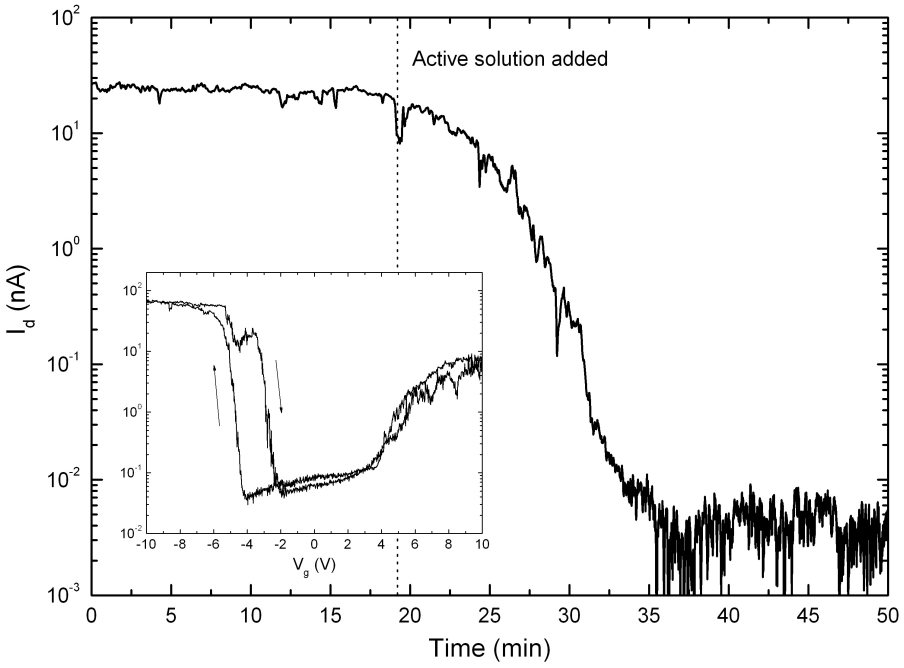

Figure 4.11: Time-dependence of doping. The gate voltage was positioned at -5 V, where CNT FET was in its ON-state on the p-type side (see inset), and the current response during the addition of 170 µM alkali solution was measured as a function of time. A clear switching from ON-state of p-type FET to OFF-state of n-type FET was noticed. Adapted from ref. [59].

The physical explanation for the observed reversal of CNT FET from p- to n-type is supposed to be the shift of the Fermi level of the nanotube, which is usually proposed to be the mechanism of alkali doping [3, 59–61]. The electrons transferred from lithium atoms via naphthalene radical to the nanotube raise the Fermi level of the nanotube from the valence-band edge to the conduction-band edge, thus changing the shape of the Schottky barrier (height and width) at the interface of the nanotube and the metal electrode (see Figure 4.12). The tunneling to the conduction band starts to dominate over the tunneling to the valence band and the type of the FET

reverts from p- to n-type.

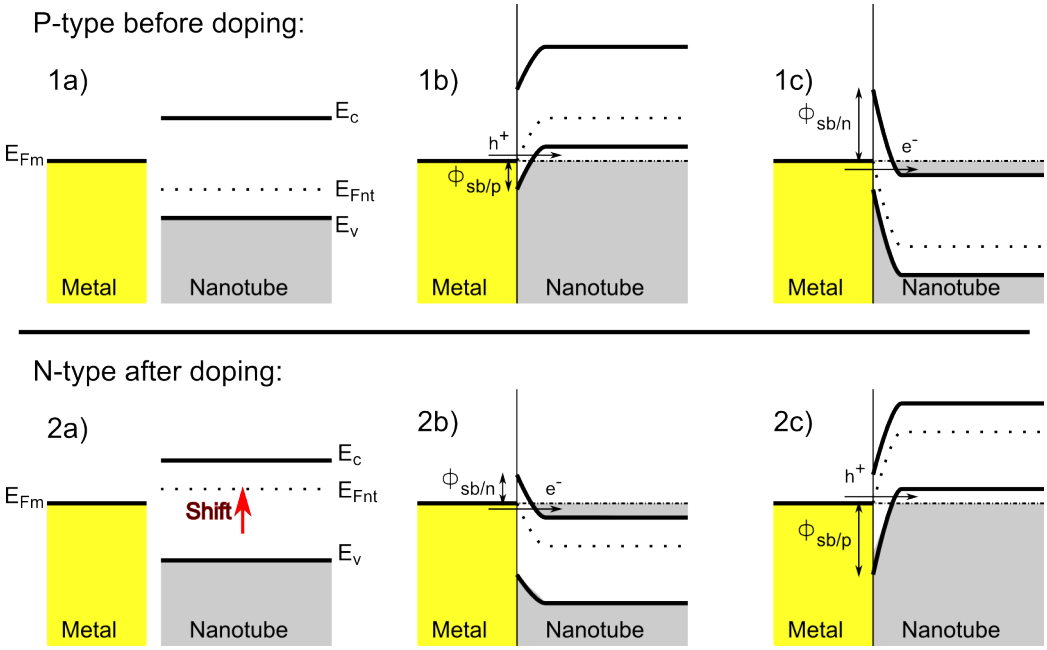

Figure 4.12: Diagrams of energy bands of the metal-nanotube contact before and after the doping. Doping shifts the Fermi level of the nanotube (E_{Fnt}) from the vicinity of the valence band (E_v) nearer to the conduction band (E_c) of the nanotube. 1a) Nonaligned energy bands before doping. 1b/1c) Schottky barrier $\Phi_{sb/p}$ for holes (h^+) is small compared to Schottky barrier $\Phi_{sb/n}$ for electrons (e^-). 2a) Nonaligned energy bands after doping. 2b) Schottky barrier $\Phi_{sb/n}$ for electrons is small compared to Schottky barrier $\Phi_{sb/p}$ for holes.

Oxygen has been proposed to cause p-type behavior of CNT FET, because the type changes from p- to n-type when oxygen is removed from the device by annealing it in vacuum [3]. Despite the vacuum pumping during the loading and low oxygen levels inside the glove box, some oxygen remained on the CNT FET when it was brought into the glove box. Thus, the noticed change of the type of CNT FET during exposure to alkali solution could be supposed to result from the reaction between lithium and oxygen which eliminates the reducing effect of oxygen. However, two studies [60, 61] demonstrate that oxygen adsorption does not affect radically the tube itself, but it tunes the work function of the electrode, which gives the asymmetric turn on to the transfer characteristics (see Figure 2.2). Oxygen adsorption does not shift the voltage range in which the conductance of FET is suppressed, whereas doping by potassium does that by shifting the Fermi level in the channel. In this study the doped

devices (e.g. device S1 in Figure 4.9) showed clear shift in the voltage range in which the conductance of the FET is suppressed, thus lithium (not oxygen) is concluded to play the main role in this doping process and causing the CNT FETs to revert from p- to n-type.

As mentioned before in chapter 1, alkali doping has been successfully done in gas-phase, where electron-beam evaporated potassium is deposited on the nanotubes reverting the type of CNT FET from p- to n-type [1–3]. This study reveals that the same effect is possible to reach by liquid-phase alkali-doping, in which alkali metal is selectively deposited at the desired places by using mild redox reactions. An inert atmosphere is needed in both methods, but liquid-phase alkali-doping is not requiring sample masking and electron beam evaporation in a vacuum chamber.

In addition to gas-phase alkali doping, some studies have been done for liquid-phase alkali doping, too. Optical absorption spectroscopy study [4] performed on thin films of carbon nanotubes show that exposure of the device to a lithium solution suppressed optical transitions between the mirror spikes in DOS. This illustrates that initially empty states of semiconducting tubes of the device are filled during exposure.The same solution was also used to modulate the electrical conductivity of the bucky paper sample [5]. These two studies perform simple measurements to networks of carbon nanotubes, so their results are averages of the behavior of many carbon nanotubes, both metallic and semiconducting. Our direct measurement of the electronic transport properties are performed just on an individual carbon nanotube and the results reveal also the effects of each component of alkali solution on the nanotube. Our study also gives more accurate information about the time dependence of the doping. Despite the differencies between the samples and the measurement methods, the results of these two studies show qualitatively similar results.

The doping process has been shown to be reversible upon exposure to oxygen, so the doped device can be returned back to p-type by bringing it outside the glove box and cleaning it with dilute HCl, distilled water and IPA. After that the doping can be repeated again (more details in reference [59]). This property along with the high sensitivity of the doped devices to oxygen could be possibly exploited for the fabrication of accurate nanoscale oxygen sensors.

The problem of stability of the doped CNT FETs in air can be solved by coating them with some airtight material. PMMA has been used for this purpose, because it is a common resist that can be easily patterned, but it has not worked very well [3]. The same group has successfully used

a thin silicon oxide layer (10 nm) for coating, and it could be rewarding to test that same material also for our alkali-doped devices.

This doping process is proposed to be unidirectional under alkali solution with respect to the concentration of the alkali solution [59]. If the process is stopped at the desired doping level, it could be possible to prepare partially doped devices such as ambipolar CNT FETs that can be used as building blocks for functional nanoelectronic devices such as voltage inverters [137]. However, more measurements are needed to prove properly this partial doping property.

The CNT FETs doped by alkali solution are not air stable, as the results reveal. However, alkali solution has an additional advantage over other n-type doping methods because it can be used to mild separation of bundled CNTs as discussed in section 2.2. By combining these two methods one can easily and inexpensively produce carbon nanotube devices with tuned electrical properties without perturbing the nanotube lattice.

Another interesting allotrope of carbon that may revolutionize the field of microelectronics is graphene [138,139]. This doping process worked well for carbon nanotubes, so it would be valuable to test it also for graphene.

Chapter 5

Conclusions

In this thesis the effects of liquid-phase alkali-doping on the electronic transport properties of individual CNT FET were studied. Originally p-type FETs were noticed to change to n-type while keeping their initial characteristics. The physical explanation for the observed reversal of CNT FET from p- to n-type is argued to be the Fermi-level shift of the nanotube. The measurements show that plain neutral naphthalene dissolved in THF has no influence on the carbon nanotube, but lithium is required for the reduction of the carbon nanotube from p- to n-type. Thus naphthalene works only as a charge transfer agent in the doping process. In addition, the sensor response of a CNT FET was tested in the liquid-phase by observing the doping process in real time. The whole doping process with a 170 µM alkali solution lasted about 160 min and ambipolar interphases between p- and n-type were observed. The attachment of lithium cations was detected with a current response of more than three orders of magnitude.

Alkali solution can be used both to separate bundled nanotubes and to tune the electronic properties of nanotubes. By combining these two properties one could get multifunctional solution for nanotube processing for nanoscale electronic devices. The high oxygen sensitivity of the doped devices is the most significant drawback of this method and some coating processes are going to be tested to overcome this problem. On the other hand, the high sensitivity of doped devices to oxygen along with the reversibility of the doping process could be possibly utilized in accurate nanoscale oxygen sensors. This doping process worked well for carbon nanotubes, so it would be nice to test it also for graphene.

Bibliography

[1] A. Javey, R. Tu, D. B. Farmer, J. Guo, R. G. Gordon, and H. Dai, High Performance n-Type Carbon Nanotube Field-Effect Transistors with Chemically Doped Contacts, *Nano Letters* **5**, 345 (2005).

[2] M. Radosavljevi, J. Appenzeller, P. Avouris, and J. Knoch, High performance of potassium n-doped carbon nanotube field-effect transistors, *American Institute of Physics* **84**, 3693 (2004).

[3] V. Derycke, R. Martel, J. Appenzeller, and P. Avouris, Carbon Nanotube Inter- and Intramolecular Logic Gates, *Nano Letters* **1**, 453 (2001).

[4] P. Petit, C. Mathis, C. Journet, and P. Bernier, Tuning and monitoring the electronic structure of carbon nanotubes, *Chemical Physics Letters* **305**, 370 (1999).

[5] E. Jouguelet, C. Mathis, and P. Petit, Controlling the electronic properties of single-wall carbon nanotubes by chemical doping, *Chemical Physics Letters* **318**, 561 (2000).

[6] T. Sorrell, *Organic chemistry*, University Science Books, 2006.

[7] P. Harris, *Carbon nanotubes and related structures: new materials for the twenty-first century*, Cambridge University Press, 2001.

[8] A. Oberlin, M. Endo, and T. Koyama, High resolution electron microscope observations of graphitized carbon fibers, *Carbon* **14**, 133 (1976).

[9] S. Iijima, Direct observation of the tetrahedral bonding in graphitized carbon black by high resolution electron microscopy, *Journal of Crystal Growth* **50**, 675 (1980).

[10] http://en.wikipedia.org/wiki/Allotropes_of_carbon, 2011.

[11] H. W. Kroto, J. R. Heath, S. C. O'brien, R. F. Curl, and R. E. Smalley, C60: Buckminsterfullerene, *Nature* **318**, 162 (1985).

[12] S. Ijima, Helical Microtubules of Graphite Carbon, *Nature* **354**, 56 (1991).

[13] S. Ijima and T. Ichihashi, Single-Shell Carbon Nanotubes of 1-nm Diameter, *Nature* **363**, 603 (1993).

[14] D. S. Bethune, C. H. Klang, M. S. de Vries, G. Gorman, R. Savoy, J. Vazquez, and R. Beyers, Cobalt Catalyzed Growth of Carbon Nanotubes with Single Atomic Layer Walls, *Nature* **363**, 605 (1993).

[15] R. van Noorden, Chemistry: The trials of new carbon, *Nature* **469**, 14 (2011).

[16] E. Joselevich, H. Dai, J. Liu, K. Hata, and A. H. Windle, Carbon Nanotube Synthesis and Organization, in *Carbon Nanotubes*, edited by M. Dresselhaus, G. Dresselhaus, and A. Jorio, volume 111 of *Topics in Applied Physics*, pp. 101–164, Springer Berlin / Heidelberg, 2008.

[17] P. J. Harris, Solid state growth mechanisms for carbon nanotubes, *Carbon* **45**, 229 (2007).

[18] H. Dai, Nanotube Growth and Characterization, in *Carbon Nanotubes*, edited by M. Dresselhaus, G. Dresselhaus, and P. Avouris, volume 80 of *Topics in Applied Physics*, pp. 29–53, Springer Berlin / Heidelberg, 2001.

[19] F. Ding, A. Rosén, and K. Bolton, Molecular dynamics study of the catalyst particle size dependence on carbon nanotube growth, *American Institute of Physics* **121**, 2775 (2004).

[20] M.-F. Yu, O. Lourie, M. J. Dyer, K. Moloni, T. F. Kelly, and R. S. Ruoff, Strength and Breaking Mechanism of Multiwalled Carbon Nanotubes Under Tensile Load, *Science* **287**, 637 (2000).

[21] A. Krishnan, E. Dujardin, T. W. Ebbesen, P. N. Yianilos, and M. M. J. Treacy, Young's modulus of single-walled nanotubes, *Physical Review B* **58**, 14013 (1998).

[22] J.-C. Charlier, X. Blase, and S. Roche, Electronic and transport properties of nanotubes, *Review of Modern Physics* **79**, 677 (2007).

[23] A. Javey, P. Qi, Q. Wang, and H. Dai, Ten- to 50-nm-long quasi-ballistic carbon nanotube devices obtained without complex lithography, *Proceedings of the National Academy of Sciences of the United States of America* **101**, 13408 (2004).

[24] J. R. Stetter and G. J. Maclay, *Carbon Nanotubes and Sensors: a Review*, pp. 357–382, Wiley-VCH Verlag GmbH, 2008.

[25] M. Zhang, S. Fang, A. A. Zakhidov, S. B. Lee, A. E. Aliev, C. D. Williams, K. R. Atkinson, and R. H. Baughman, Strong, Transparent, Multifunctional, Carbon Nanotube Sheets, *Science* **309**, 1215 (2005).

[26] L. S. Schadler, S. C. Giannaris, and P. M. Ajayan, Load transfer in carbon nanotube epoxy composites, *American Institute of Physics* **73**, 3842 (1998).

[27] H. Dai, J. H. Hafner, A. G. Rinzler, D. T. Colbert, and R. E. Smalley, Nanotubes as nanoprobes in scanning probe microscopy, *Nature* **384**, 147 (1996).

[28] A. C. Dillon, K. M. Jones, T. A. Bekkedahl, C. H. Kiang, D. S. Bethune, and M. J. Heben, Storage of hydrogen in single-walled carbon nanotubes, *Nature* **386**, 377 (1997).

[29] R. Saito, G. Dresselhaus, and M. Dresselhaus, *Physical properties of carbon nanotubes*, Imperial College Press, 1998.

[30] M. Wilson, Electrons in Atomically Thin Carbon Sheets Behave Like Massless Particles, *American Institute of Physics* **59**, 21 (2006).

[31] R. Saito, G. Dresselhaus, and M. S. Dresselhaus, Trigonal warping effect of carbon nanotubes, *Physical Review B* **61**, 2981 (2000).

[32] J. W. Mintmire and C. T. White, Universal Density of States for Carbon Nanotubes, *Physical Review Letters* **81**, 2506 (1998).

[33] J. Svensson, *Carbon nanotube transistors: nanotube growth, contact properties and novel devices*, PhD thesis, University of Gothenburg, 2010.

[34] Y. Imry and R. Landauer, Conductance viewed as transmission, *Review of Modern Physics* **71**, S306 (1999).

[35] M. S. Purewal, B. H. Hong, A. Ravi, B. Chandra, J. Hone, and P. Kim, Scaling of Resistance and Electron Mean Free Path of Single-Walled Carbon Nanotubes, *Physical Review Letters* **98**, 186808 (2007).

[36] A. Javey, J. Guo, Q. Wang, M. Lundstrom, and H. Dai, Ballistic carbon nanotube field-effect transistors, *Nature* **424**, 654 (2003).

[37] R. Martel, T. Schmidt, H. R. Shea, T. Hertel, and P. Avouris, Single- and multi-wall carbon nanotube field-effect transistors, *Applied Physics Letters* **73**, 2447 (1998).

[38] S. Rosenblatt, Y. Yaish, J. Park, J. Gore, V. Sazonova, and P. L. McEuen, High Performance Electrolyte Gated Carbon Nanotube Transistors, *Nano Letters* **2**, 869 (2002).

[39] P. Avouris, Z. Chen, and V. Perebeinos, Carbon-based electronics, *Nature Nano* **2**, 605 (2007).

[40] G. Moore, Cramming More Components Onto Integrated Circuits, *Electronics* **38** (1965).

[41] ITRS, International technology roadmap for semiconductors: Process, integration, devices, and structures., Technical report, 2009.

[42] T. Dürkop, S. A. Getty, E. Cobas, and M. S. Fuhrer, Extraordinary Mobility in Semiconducting Carbon Nanotubes, *Nano Letters* **4**, 35 (2004).

[43] R. V. Seidel, A. P. Graham, J. Kretz, B. Rajasekharan, G. S. Duesberg, M. Liebau, E. Unger, F. Kreupl, and W. Hoenlein, Sub-20 nm Short Channel Carbon Nanotube Transistors, *Nano Letters* **5**, 147 (2005).

[44] A. Javey, H. Kim, M. Brink, Q. Wang, J. Ural, Antand Guo, P. McIntyre, P. McEuen, M. Lundstrom, and H. Dai, High-kappa dielectrics for advanced carbon-nanotube transistors and logic gates, *Nature Materials* **1**, 241 (2002).

[45] R. Smith, Electronics: circuits and devices, USA, 1987.

[46] J. Millman and A. Grabel, Microelectronics, USA, 1987.

[47] S. J. Tans, A. R. M. Verschueren, and C. Dekker, Room-temperature transistor based on a single carbon nanotube, *Nature* **393** (1998).

[48] W. Schottky, Abweichungen vom Ohmschen Gesets in Halbleitern, *Phys. Z.* **41**, 570 (1940).

[49] C. Kittel, Introduction to Solid State Physics, USA, 2005.

[50] S. Sze and K. Ng, *Physics of semiconductor devices*, Wiley-Interscience publication, Wiley-Interscience, 2007.

[51] R. T. Tung, Recent advances in Schottky barrier concepts, *Materials Science and Engineering: R: Reports* **35**, 1 (2001).

[52] J. Tersoff, Schottky Barrier Heights and the Continuum of Gap States, *Physical Review Letters* **52**, 465 (1984).

[53] Y. Xue and S. Datta, Fermi-Level Alignment at Metal-Carbon Nanotube Interfaces: Application to Scanning Tunneling Spectroscopy, *Physical Review Letters* **83**, 4844 (1999).

[54] J. Colinge and C. Colinge, *Physics of semiconductor devices*, Kluwer Academic Publishers, 2002.

[55] F. Léonard and J. Tersoff, Role of Fermi-Level Pinning in Nanotube Schottky Diodes, *Physical Review Letters* **84**, 4693 (2000).

[56] F. m. c. Léonard and A. A. Talin, Size-Dependent Effects on Electrical Contacts to Nanotubes and Nanowires, *Physical Review Letters* **97**, 026804 (2006).

[57] M. Biercuk, S. Ilani, C. Marcus, and P. Mceuen, Electrical transport in single-wall carbon nanotubes, in *Carbon nanotubes*, edited by A. Jorio, G. Dresselhaus, and M. Dresselhaus, volume 111 of *Topics in Applied Physics*, pp. 455–493, Springer, Berlin, 2008.

[58] Z. Chen, J. Appenzeller, J. Knoch, Y.-m. Lin, and P. Avouris, The Role of Metal-Nanotube Contact in the Performance of Carbon Nanotube Field-Effect Transistors, *Nano Letters* **5**, 1497 (2005), PMID: 16178264.

[59] P. Yotprayoonsak, K. Hannula, T. Lahtinen, M. Ahlskog, and A. Johansson, Liquid-phase alkali-doping of individual carbon nanotube field-effect transistors observed in real-time, *Carbon* **49**, 5283 (2011).

[60] S. Heinze, J. Tersoff, R. Martel, V. Derycke, J. Appenzeller, and P. Avouris, Carbon Nanotubes as Schottky Barrier Transistors, *Physical Review Letters* **89**, 106801 (2002).

[61] V. Derycke, R. Martel, J. Appenzeller, and P. Avouris, Controlling doping and carrier injection in carbon nanotube transistors, *American Institute of Physics* **80**, 2773 (2002).

[62] P. Liu, Q. Sun, F. Zhu, K. Liu, K. Jiang, L. Liu, Q. Li, and S. Fan, Measuring the Work Function of Carbon Nanotubes with Thermionic Method, *Nano Letters* **8**, 647 (2008), PMID: 18225940.

[63] Z. Zhang, X. Liang, S. Wang, K. Yao, Y. Hu, Y. Zhu, Q. Chen, W. Zhou, Y. Li, Y. Yao, J. Zhang, and L.-M. Peng, Doping-Free Fabrication of Carbon Nanotube Based Ballistic CMOS Devices and Circuits, *Nano Letters* **7**, 3603 (2007).

[64] J. Appenzeller, J. Knoch, V. Derycke, R. Martel, S. Wind, and P. Avouris, Field-Modulated Carrier Transport in Carbon Nanotube Transistors, *Physical Review Letters* **89**, 126801 (2002).

[65] J. Appenzeller, M. Radosavljević, J. Knoch, and P. Avouris, Tunneling Versus Thermionic Emission in One-Dimensional Semiconductors, *Physical Review Letters* **92**, 048301 (2004).

[66] Y.-M. Lin, J. Appenzeller, J. Knoch, and P. Avouris, High-performance carbon nanotube field-effect transistor with tunable polarities, *Nanotechnology, IEEE Transactions on* **4**, 481 (2005).

[67] J. Leppäniemi, Multi-walled carbon nanotubes as field-effect transistors, Master's thesis, Department of Physics, Jyväskylä University, Jyväskylä, Finland, 2008.

[68] P. Avouris, Z. Chen, and V. Perebeinos, Carbon-based electronics, *Nature Nano* **2**, 605 (2007).

[69] J. Appenzeller, Y.-M. Lin, J. Knoch, and P. Avouris, Band-to-Band Tunneling in Carbon Nanotube Field-Effect Transistors, *Physical Review Letters* **93**, 196805 (2004).

[70] C. W. Lee, X. Dong, S. H. Goh, J. Wang, J. Wei, and L.-J. Li, Illumination-Enhanced Hysteresis of Transistors Based on Carbon Nanotube Networks, *The Journal of Physical Chemistry C* **113**, 4745 (2009).

[71] M. Rinkiö, A. Johansson, M. Zavodchikova, J. Toppari, G. Albert, A. Nasibulin, E. Kauppinen, and P. Törmä, High-Yield of Memory Elements from Carbon Nanotube Field-Effect Transistors with Atomic Layer Deposited Gate Dielectric, *New Journal Physics* **10**, 103019 (2008).

[72] M. H. Yang, K. B. K. Teo, L. Gangloff, W. I. Milne, D. G. Hasko, Y. Robert, and P. Legagneux, Advantages of top-gate, high-k dielectric carbon nanotube field-effect transistors, *Applied Physics Letters* **88**, 113507 (2006).

[73] W. Kim, A. Javey, O. Vermesh, Q. Wang, Y. Li, and H. Dai, Hysteresis Caused by Water Molecules in Carbon Nanotube Field-Effect Transistors, *Nano Letters* **3**, 193 (2003).

[74] D. Sung, S. Hong, Y.-H. Kim, N. Park, S. Kim, S. L. Maeng, and K.-C. Kim, Ab initio study of the effect of water adsorption on the carbon nanotube field-effect transistor, *American Institute of Physics* **89**, 243110 (2006).

[75] J. S. Lee, S. Ryu, K. Yoo, I. S. Choi, W. S. Yun, and J. Kim, Origin of Gate Hysteresis in Carbon Nanotube Field-Effect Transistors, *The Journal of Physical Chemistry C* **111**, 12504 (2007).

[76] H. G. Ong, J. W. Cheah, X. Zou, B. Li, X. H. Cao, H. Tantang, L.-J. Li, H. Zhang, G. C. Han, and J. Wang, Origin of hysteresis in the transfer characteristic of carbon nanotube field effect transistor, *Journal of Physics D: Applied Physics* **44**, 285301 (2011).

[77] A. J. S. Ahammad, J.-J. Lee, and M. A. Rahman, Electrochemical Sensors Based on Carbon Nanotubes, *Sensors* **9**, 2289 (2009).

[78] F. Patolsky, G. Zheng, O. Hayden, M. Lakadamyali, X. Zhung, and C. Lieber, Electrical detection of single viruses, *Proceedings of the National Academy of Sciences of the United States of America* **101**, 14017 (2004).

[79] P. Hu, J. Zhang, L. Li, Z. Wang, W. O'Neill, and P. Estrela, Carbon Nanostructure-Based Field-Effect Transistors for Label-Free Chemical/Biological Sensors, *Sensors* **10**, 5133 (2010).

[80] S. Peng and K. Cho, Ab Initio Study of Doped Carbon Nanotube Sensors, *Nano Letters* **3**, 513 (2003).

[81] S. Boussaad, N. J. Tao, R. Zhang, T. Hopson, and L. A. Nagahara, In situ detection of cytochrome c adsorption with single walled carbon nanotube device, *Chemical Communications* , 1502 (2003).

[82] A. B. Artyukhin, M. Stadermann, R. W. Friddle, P. Stroeve, O. Bakajin, and A. Noy, Controlled Electrostatic Gating of Carbon Nanotube FET Devices, *Nano Letters* **6**, 2080 (2006).

[83] E. L. Gui, L.-J. Li, K. Zhang, Y. Xu, X. Dong, X. Ho, P. S. Lee, J. Kasim, Z. X. Shen, J. A. Rogers, and Mhaisalkar, DNA Sensing by Field-Effect Transistors Based on Networks of Carbon Nanotubes, *Journal of the American Chemical Society* **129**, 14427 (2007).

[84] K. Besteman, J.-O. Lee, F. G. M. Wiertz, H. A. Heering, and C. Dekker, Enzyme-Coated Carbon Nanotubes as Single-Molecule Biosensors, *Nano Letters* **3**, 727 (2003).

[85] E. L. Gui, L.-J. Li, K. Zhang, Y. Xu, X. Dong, X. Ho, P. S. Lee, J. Kasim, Z. X. Shen, J. A. Rogers, and Mhaisalkar, DNA Sensing by Field-Effect Transistors Based on Networks of Carbon Nanotubes, *Journal of the American Chemical Society* **129**, 14427 (2007).

[86] R. J. Chen, H. C. Choi, S. Bangsaruntip, E. Yenilmez, X. Tang, Q. Wang, Y.-L. Chang, and H. Dai, An Investigation of the Mechanisms of Electronic Sensing of Protein Adsorption on Carbon Nanotube Devices, *Journal of the American Chemical Society* **126**, 1563 (2004).

[87] H. R. Byon and H. C. Choi, Network Single-Walled Carbon Nanotube-Field Effect Transistors (SWNT-FETs) with Increased

Schottky Contact Area for Highly Sensitive Biosensor Applications, *Journal of the American Chemical Society* **128**, 2188 (2006).

[88] D. S. Hecht, R. J. A. Ramirez, M. Briman, E. Artukovic, K. S. Chichak, J. F. Stoddart, and G. Grüner, Bioinspired Detection of Light Using a Porphyrin-Sensitized Single-Wall Nanotube Field Effect Transistor, *Nano Letters* **6**, 2031 (2006).

[89] A. Maroto, K. Balasubramanian, M. Burghard, and K. Kern, Functionalized Metallic Carbon Nanotube Devices for pH Sensing, *ChemPhysChem* **8**, 220 (2007).

[90] I. Heller, A. M. Janssens, J. Mannik, E. D. Minot, S. G. Lemay, and C. Dekker, Identifying the Mechanism of Biosensing with Carbon Nanotube Transistors, *Nano Letters* **8**, 591 (2008).

[91] N. Peng, Q. Zhang, C. L. Chow, O. K. Tan, and N. Marzari, Sensing Mechanisms for Carbon Nanotube Based NH3 Gas Detection, *Nano Letters* **9**, 1626 (2009).

[92] T. H. Kim, J. Lee, and S. Hong, Highly Selective Environmental Nanosensors Based on Anomalous Response of Carbon Nanotube Conductance to Mercury Ions, *The Journal of Physical Chemistry C* **113**, 19393 (2009).

[93] M. Glerup, V. Krstic, C. Ewels, M. Holzinger, and G. V. Lier, Doping of Carbon Nanotubes, in *Doped Nanomaterials and Nanodevices*, edited by W. Chen, volume 3 of *Nanotechnology book series*, American Scientific Publishers, USA, 2010.

[94] C. Dekker, Carbon nanotubes as molecular quantum wires, *Physics Today* **52** (1999).

[95] J.-C. Charlier, M. Terrones, M. Baxendale, V. Meunier, T. Zacharia, N. L. Rupesinghe, W. K. Hsu, N. Grobert, H. Terrones, and G. A. J. Amaratunga, Enhanced Electron Field Emission in B-doped Carbon Nanotubes, *Nano Letters* **2**, 1191 (2002).

[96] L. Bulusheva, A. Okotrub, A. Kurenya, H. Zhang, H. Zhang, X. Chen, and H. Song, Electrochemical properties of nitrogen-doped carbon nanotube anode in Li-ion batteries, *Carbon* **49**, 4013 (2011).

[97] F. Villalpando-Páez, A. H. Romero, E. Muñoz-Sandoval, L. M. Martínez, H. Terrones, and M. Terrones, Fabrication of vapor and gas sensors using films of aligned CNx nanotubes, *Chemical Physics Letters* **386**, 137 (2004).

[98] K. Jiang, L. S. Schadler, R. W. Siegel, X. Zhang, H. Zhang, and M. Terrones, Protein immobilization on carbon nanotubes via a two-step process of diimide-activated amidation, *Journal of Materials Chemistry* **14**, 37 (2004).

[99] O. Stephan, P. M. Ajayan, C. Colliex, P. Redlich, J. M. Lambert, P. Bernier, and P. Lefin, Doping Graphitic and Carbon Nanotube Structures with Boron and Nitrogen, *Science* **266**, 1683 (1994).

[100] U. Bangert, A. Bleloch, M. H. Gass, A. Seepujak, and J. van den Berg, Doping of few-layered graphene and carbon nanotubes using ion implantation, *Physical Review B* **81**, 245423 (2010).

[101] M. Terrones, A. Filho, and A. Rao, Doped Carbon Nanotubes: Synthesis, Characterization and Applications, in *Carbon Nanotubes*, edited by M. Dresselhaus, G. Dresselhaus, and A. Jorio, volume 111 of *Topics in Applied Physics*, pp. 531–566, Springer Berlin / Heidelberg, 2008.

[102] M. Dresselhaus and G. Dresselhaus, Intercalation compounds of graphite, *Advances in Physics* **30**, 139 (1981).

[103] M. R. Pederson and J. Q. Broughton, Nanocapillarity in fullerene tubules, *Physical Review Letters* **69**, 2689 (1992).

[104] D. Ugarte, T. Stöckli, J. Bonard, A. Châtelain, and W. de Heer, Filling carbon nanotubes, *Applied Physics A: Materials Science & Processing* **67**, 101 (1998), 10.1007/s003390050744.

[105] L.-J. Li, A. N. Khlobystov, J. G. Wiltshire, G. A. D. Briggs, and R. J. Nicholas, Diameter-selective encapsulation of metallocenes in single-walled carbon nanotubes, *Nature Materials* **4**, 481 (2005).

[106] D. Guldi and N. Martín, *Carbon Nanotubes and Related Structures: Synthesis, Characterization, Functionalization, and Applications*, Wiley-VCH, 2010.

[107] M. Cha, S. Jung, M.-H. Cha, G. Kim, J. Ihm, and J. Lee, Reversible Metal-Semiconductor Transition of ssDNA-Decorated Single-Walled Carbon Nanotubes, *Nano Letters* **9**, 1345 (2009).

[108] R. Martel, Sorting Carbon Nanotubes for Electronics, *ACS Nano* **2**, 2195 (2008).

[109] P. W. Chiu, G. S. Duesberg, U. Dettlaff-Weglikowska, and S. Roth, Interconnection of carbon nanotubes by chemical functionalization, **80**, 3811 (2002).

[110] K. Kim, D. Bae, J. Kim, K. Park, S. Lim, J.-J. Kim, W. Choi, C. Park, and Y. Lee, Modification of Electronic Structures of a Carbon Nanotube by Hydrogen Functionalization, *Advanced Materials* **14**, 1818 (2002).

[111] E. Mickelson, C. Huffman, A. Rinzler, R. Smalley, R. Hauge, and J. Margrave, Fluorination of single-wall carbon nanotubes, *Chemical Physics Letters* **296**, 188 (1998).

[112] L. Ding, S. Wang, Z. Zhang, Q. Zeng, Z. Wang, T. Pei, L. Yang, X. Liang, J. Shen, Q. Chen, R. Cui, Y. Li, and L.-M. Peng, Y-Contacted High-Performance n-Type Single-Walled Carbon Nanotube Field-Effect Transistors: Scaling and Comparison with Sc-Contacted Devices, *Nano Letters* **9**, 4209 (2009).

[113] N. Moriyama, Y. Ohno, T. Kitamura, S. Kishimoto, and T. Mizutani, Change in carrier type in high- k gate carbon nanotube field-effect transistors by interface fixed charges, *Nanotechnology* **21**, 165201 (2010).

[114] K. Hannula, Separating Bundled Single-Wall Carbon nanotubes, Bachelor's thesis, 2009, Department of Physics, Jyväskylä University, Jyväskylä, Finland.

[115] M. S. Dresselhaus and M. Endo, Relation of Carbon Nanotubes to Other Carbon Materials, in *Carbon Nanotubes*, edited by M. Dresselhaus, G. Dresselhaus, and P. Avouris, volume 80 of *Topics in Applied Physics*, pp. 11–28, Springer Berlin / Heidelberg, 2001.

[116] R. Martel, Sorting Carbon Nanotubes for Electronics, *ACS Nano* **2**, 2195 (2008).

[117] A. Pénicaud, P. Poulin, A. Derré, E. Anglaret, and P. Petit, Spontaneous Dissolution of a Single-Wall Carbon Nanotube Salt, *Journal of the American Chemical Society* **127**, 8 (2005).

[118] M. Inagaki and O. Tanaike, Host effect on the formation of sodium-tetrahydrofuran-graphite intercalation compounds, *Synthetic Metals* **73**, 77 (1995).

[119] M. Yus, R. P. Herrera, and A. Guijarro, On the mechanism of the naphthalene-catalysed lithiation: the role of the naphthalene dianion, *Tetrahedron Letters* **42**, 3455 (2001).

[120] J. Smid, A Stable Dianion of Naphthalene, *Journal of the American Chemical Society* **87**, 655 (1965).

[121] J. F. Garst, Electron transfer, naphthalene radical anion, and alkyl halides, *Accounts of Chemical Research* **4**, 400 (1971).

[122] P. P. H. Sternberg, C. Donne, On the Solubilization of Coal via Reductive alkylation, *The ACS Division of Fuel Chemistry: Preprints* **14**, 87 (1970).

[123] G. May and C. Spanos, *Fundamentals of semiconductor manufacturing and process control*, IEEE, 2006.

[124] B. Bhushan, *Handbook of nanotechnology*, Gale virtual reference library, Springer, 2007.

[125] http://www.microchem.com/products/pdf/PMMA_Data_Sheet.pdf, 2011.

[126] https://www.jyu.fi/science/muut_yksikot/nsc/en/research/facilities/instruments/details/e_line, 2011.

[127] http://www.nanocyl.com/en/Products-Solutions/Products/Research-Grades/Single-Wall-Carbon-Nanotubes, 2011.

[128] K. Lu, R. Lago, Y. Chen, M. Green, P. Harris, and S. Tsang, Mechanical damage of carbon nanotubes by ultrasound, *Carbon* **34**, 814 (1996).

[129] Z. Chen and M. Hojo, Relationship between Triple Ion Formation Constants and the Salt Concentration of the Minimum in the Conductometric Curves in Low-Permittivity Solvents, *The Journal of Physical Chemistry B* **101**, 10896 (1997).

[130] H. Weingärtner, V. C. Weiss, and W. Schröer, Ion association and electrical conductance minimum in Debye-Hückel-based theories of the hard sphere ionic fluid, *American Institute of Physics* **113**, 762 (2000).

[131] T. Kar, J. Pattanayak, and S. Scheiner, Insertion of Lithium Ions into Carbon Nanotubes: An ab Initio Study, *The Journal of Physical Chemistry A* **105**, 10397 (2001).

[132] V. Meunier, J. Kephart, C. Roland, and J. Bernholc, Ab Initio Investigations of Lithium Diffusion in Carbon Nanotube Systems, *Physical Review Letters* **88**, 075506 (2002).

[133] K. Nishidate and M. Hasegawa, Energetics of lithium ion adsorption on defective carbon nanotubes, *Physical Review B* **71**, 245418 (2005).

[134] A. G. Cano-Márquez, F. J. Rodríguez-Macías, J. Campos-Delgado, C. G. Espinosa-González, F. Tristán-López, D. Ramírez-González, D. A. Cullen, D. J. Smith, M. Terrones, and Y. I. Vega-Cantú, Ex-MWNTs: Graphene Sheets and Ribbons Produced by Lithium Intercalation and Exfoliation of Carbon Nanotubes, *Nano Letters* **9**, 1527 (2009).

[135] P. G. Collins, K. Bradley, M. Ishigami, and A. Zettl, Extreme Oxygen Sensitivity of Electronic Properties of Carbon Nanotubes, *Science* **287**, 1801 (2000).

[136] A. Star, T.-R. Han, J.-C. P. Gabriel, K. Bradley, and G. Grüner, Interaction of Aromatic Compounds with Carbon Nanotubes: Correlation to the Hammett Parameter of the Substituent and Measured Carbon Nanotube FET Response, *Nano Letters* **3**, 1421 (2003).

[137] A. Javey, M. Shim, and H. Dai, Electrical properties and devices of large-diameter single-walled carbon nanotubes, *American Institute of Physics* **80**, 1064 (2002).

[138] A. K. Geim and K. S. Novoselov, The rise of graphene, *Nature Materials* **6**, 183 (2007).

[139] K. Kim, J.-Y. Choi, T. Kim, S.-H. Cho, and H.-J. Chung, A role for graphene in silicon-based semiconductor devices, *Nature* **479**, 338 (2011).

Appendix A

Prepared Devices

Here is additional information of the chips on which the devices mentioned in the text are. During this work, CNT FETs were started to prepare on more than twenty chips. The fabrication process of CNT FETs consists of many steps, thus failure in one step means that the chip is not useful anymore. For example, there may be too much tubes on the chip after deposition, so that individual tubes cannot be used for devices. Metallization can also fail and sometimes all the electrodes are connected together.

Device number	Nanotube diameter (nm)	Channel length (µm)	Metallic or semiconducting	Type before doping	Type after doping	Abbreviation
1	0,7	400	-	-	-	
2	0,7	300	-	-	-	
3	1,0	170	m	-	-	
4	2,0	340	-	-	-	
5	1,5	240	sc	p	-	
6	2,0	200	m	-	-	
7	0,6	230	-	-	-	
8	1,0	80	-	-	-	
9	1,4	290	sc	p	Shifted p	
10	1,5	160	sc	p/ambip.	n/ambip.	S3

Table A.1: CNT FETs on the chip called KH_NC_ox500_01. Character "-" means that the value in question is not determined.

Device number	Nanotube diameter (nm)	Channel length (µm)	Metallic or semicon-ducting	Type before doping	Type after doping	Abbreviation
1	2,0	390	m	-	-	
2	3,2	310	m	-	-	
3.1	1,5	930	sc	p	-	
3.2	1,5	470	sc	p	n	S2
4	1,9	270	m	-	-	
5	2,1	300	sc	p/ambip.	n/ambip.	S1
6	1,3	320	m	-	-	
7	2,1	510	m	-	-	
8	2,5	330	-	-	-	
9	2,6	590	-	-	-	
10	-	330	-	-	-	
11	1,2	400	sc	p/ambip.	-	
12	1,1	530	-	-	-	
13	1,7	540	m	-	-	
14	3,6	380	m	-	-	

Table A.2: CNT FETs on the chip KH_NC_ox500_05. The channel length of the device 5 is measured with AFM, other channel lengths are measured from the designed overlay pattern.